Taylor & Francis
Taylor & Francis Group

RESEARCH ARTICLE

Check for updates

Circ-0000953 deficiency exacerbates podocyte injury and autophagy disorder by targeting Mir665-3p-Atg4b in diabetic nephropathy

Xueqi Liu[a]*, Ling Jiang[a]*, Hanxu Zeng[a]*, Li Gao[a]*, Shanshan Guo[a], Chaoyi Chen[a], Xinran Liu[a], Mengya Zhang[a], Lijuan Ma[a], Yuanyuan Li[a], Xiangming Qi[a], and Yonggui Wu [a,b]

[a]Department of Nephropathy, the First Affiliated Hospital of Anhui Medical University, Hefei, Anhui, PR China; [b]Center for Scientific Research, Anhui Medical University, Hefei, Anhui, PR China

ABSTRACT

Circular RNAs (circRNAs) are special non-coding RNA (ncRNA) molecules that play a significant role in many diseases. However, the biogenesis and regulation of circRNAs in diabetic nephropathy (DN) are largely unknown. Here, we investigated the expression profile of circRNAs in kidney of DN mice through circular RNA sequencing (circRNA-seq). The renal biopsy samples of patients with DN had low circ -0,000,953 expression, which was significantly associated with renal function. Furthermore, loss-of-function and gain-of-function experiments were carried out to prove the role of circ -0,000,953 in DN. Podocyte conditional knockin (cKI) or systemic overexpression of circ -0,000,953 alleviated albuminuria and restored macroautophagy/autophagy in kidney of diabetic mice. However, circ -0,000,953 knockdown exacerbated albuminuria and podocyte injury. Mechanistically, we found circ -0,000,953 directly binds to Mir665-3p-Atg4b to perform its function. Silencing of Mir665-3p or over-expression of Atg4b recovered podocyte autophagy both in vitro and in vivo. To examine the cause of circ -0,000,953 downregulation in DN, bioinformatics prediction found that circ -0,000,953 sequence has a high possibility of containing an m6A methylation site. Additionally, METTL3 was proved to regulate the expression and methylation level of circ -0,000,953 through YTHDF2 (YTH N6-methyladenosine RNA binding protein 2). In conclusion, this study revealed that circ -0,000,953 regulates podocyte autophagy by targeting Mir665-3p-Atg4b in DN. Therefore, circ -0,000,953 is a potential biomarker for prevention and cure of DN.

Abbreviation: CCL2/MCP-1: C-C motif chemokine ligand 2; ceRNA: competing endogenous RNA; circRNA: circular RNA; cKI: conditional knockin; cKO: conditional knockout; CRE: creatinine; DM: diabetes mellitus; DN: diabetic nephropathy; ESRD: end-stage renal disease; HG: high glucose; IF: immunofluorescence; MAP1LC3/LC3B: microtubule-associated protein 1 light chain 3 beta; MPC5: mouse podocyte clone 5; MTECs: mouse tubular epithelial cells; MTOR: mechanistic target of rapamycin kinase; NC: normal control; ncRNA: non-coding RNA; NPHS1: nephrosis 1, nephrin; NPHS2: nephrosis 2, podocin; PAS: periodic acid-Schiff; RELA/p65: v-rel reticuloendotheliosis viral oncogene homolog A (avian); SDs: slit diaphragm proteins; Seq: sequencing; STZ: streptozotocin; SV40: SV40-MES13-cells, mouse mesangial cell line; T1D: type 1 diabetes mellitus; T2D: type 2 diabetes mellitus; TEM: transmission electron microscopy; TNF/TNF-α: tumor necrosis factor; VECs: vascular endothelial cells; WT1: WT1 transcription factor; YTHDF2: YTH N6-methyladenosine RNA binding protein 2.

Introduction

Diabetic nephropathy (DN) is the most common complication in patients with diabetes [1]. At present, effective therapeutic strategies for DN are lacking. The pathogenesis and treatment of DN have been a major focus of research worldwide [2]. Exfoliation and death of podocytes, compensatory hypertrophy of surviving podocytes and podocyte fusion are some of the most important pathological changes in the early stage of DN, and podocyte injury-induced proteinuria can lead to the continuous progression of DN [3].

Autophagy is a process in which eukaryotic cells use lysosomes to degrade their own cytoplasmic proteins and damaged organelles to maintain cell homeostasis [4–7]. Autophagy is divided into three types, including macroautophagy, microautophagy, and chaperone-mediated autophagy. Recent research shows that autophagy is a self-protective mechanism of podocytes in the progression of DN [8–12]. Autophagy can resist a variety of pathological injury factors. If autophagy is impaired, podocyte injury and albuminuria will be caused, which further aggravates glomerulosclerosis [13–15]. Therefore, it is necessary to understand the specific mechanism underlying podocyte damage in DN and formulate effective prevention strategies [16,17].

Circular RNAs (circRNAs) are novel endogenous non-coding RNAs (ncRNAs) discovered recently, which have attracted significant interest from researchers worldwide [18]. They are mainly formed through reverse splicing of exons or introns and occur as a covalent closed loop [19]. The closed-loop structure of circRNAs prevent their degradation by exonucleases and

are more stable than the linear structure [20]. CircRNAs are sequentially conserved, mainly located in the cytoplasm or stored in exosomes, and play a regulatory role at the transcriptional or post-transcriptional level [21]. They perform various regulatory functions by acting as miRNA sponges or competing endogenous RNAs (ceRNAs), controlling the expression of parental genes and directly binding to proteins to affect their functions; additionally, a small number of circRNAs can be translated into proteins [22]. Recently, research reports that circRNAs play a crucial role in occurrence and progression of various diseases, including cancer, diabetes and cardiovascular disease. However, the biogenesis and regulation of circRNAs in DN are largely unknown [23].

Therefore, in the present study, we investigated the effect of *circ -0,000,953* in experimental DN and explored the mechanism of *circ -0,000,953-Mir665-3p-Atg4b-* mediated autophagy in diabetes-injured podocytes. We showed that METTL3 regulated the expression and methylation level of *circ -0,000,953* through YTHDF2 (YTH N6-methyladenosine RNA binding protein 2). Altogether, this study revealed that *circ -0,000,953* deficiency exacerbates podocyte injury and reduces autophagy through *Mir665-3p-Atg4b* in DN.

Results

Circ -0,000,953 *was downregulated in DN mice and patients and METTL3 mediated the m6A methylation of* circ -0,000,953

To examine the expression profile of circRNAs associated with DN, the renal cortex tissues were collected for high-throughput circRNA-seq. Diabetes mice was induced by STZ for 12 weeks. Albuminuria, kidney weight:body weight, and blood glucose levels were significantly increased in diabetic mice (Figures S1A–C). PAS staining indicated that the degree of mesangial dilatation and tubulointerstitial injury was alleviated in mice with STZ-induced diabetes (Figure S1D). Heat map demonstrated the top 20 differentially expressed circRNAs with high degrees of homology (Figure 1A). The distribution and composition of differentially expressed circRNAs were shown in Figure 1B. Furthermore, real-time PCR revealed the top 20 markedly expressed circRNAs. The results proved that *circ -0,000,953* expression was found to be significantly downregulated in mice with DN ($P = 0.0007$) (Figure 1C). We further detected the expression of *circ -0,000,953* on T2D mice like db/db mice, ob/ob mice and high-fat diet (HFD) mice, the results showed that *circ -0,000,953* was down-regulated in the kidney of T2D mice (Figure 1D). Additionally, the expression of *circ -0,000,953* was examined in innate kidney cells, including renal tubular epithelial cells (MTECs), mouse podocyte clone 5 (MPC5), mesangial cells (SV40 cells) and vascular endothelial cells (VECs). We discovered that *circ -0,000,953* expression was significantly downregulated in HG-stimulated podocytes (Figure 1E). FISH assay revealed that *circ -0,000,953* predominantly localized in the cytoplasm of podocytes (Figure 1F). The correlation between *circ -0,000,953* expression was examined by FISH assay (Figure 1G). *Circ -0,000,953* expression was found to be significantly downregulated in patients with

both T1D and T2D. Additionally, it was negatively correlated with 24 h urinary microalbumin levels and serum creatinine (CRE) levels and positively correlated with estimated glomerular filtration rate (eGFR) in DN patients (Figure 1H).

Recent studies have reported that circRNAs have more abundant m6A modifications [24]. In our previous study, we demonstrated that METTL3-mediated m6A methylation regulated podocyte injury in DN [2]. However, whether METTL3 regulates m6A methylation of circRNAs in DN remains unclear. Methylation modification sites near the termination codon of *circ -0,000,953* were examined using SRAMP (http://www.cuilab.cn/sramp) (Figure 1I). Podocyte conditional knockout (cKO) of *Mettl3* restored *circ -0,000,953* expression in diabetic mice (Figure 1J). MeRIP-qPCR revealed that compared with the IgG group, the m6A antibody significantly enriched *circ -0,000,953* after HG stimulation; however, *mettl3*-cKO reduced the enrichment of anti-m6A antibody in *circ -0,000,953* (Figure 1K). FISH assay revealed that *circ -0,000,953* was enhanced in *mettl3*-KO podocytes (Figure 1L). Additionally, the results revealed that silencing of *Ythdf2* supressed the degradation of *circ -0,000,953* (Figure 1M,N).

Characterization of circ -0,000,953

In this study, *circ -0,000,953* (*mmu_circ_0000953*) derived from the parental gene *R3hcc1l/D19Ertd386e* was characterized. *Circ -0,000,953* is located on chromosome 19: 42637041–42638831. The genomic structure of *circ -0,000,953* suggested that it consisted of 1 exon (exon 2) from the *R3hcc1l* gene locus (Figure S1E). As shown in Figure S1F, the PCR product of *circ -0,000,953* was found to involve head-to-tail splicing and matched the sequence displayed for *circ -0,000,953* in circBase (http://circbase.org/) as examined via sanger sequencing. Because a head-to-tail splicing product may be derived from genomic rearrangements or trans-splicing, we examined the resistance of *circ -0,000,953* to digestion by Rnase R (Figure S1G), a highly processive 3′-5′ exonuclease, to validate the stability of *circ -0,000,953*. The results revealed that the expression of *circ -0,000,953* did not change markedly under the action of Rnase R, while the parental gene *R3hcc1l* decreased significantly. Furthermore, when the transcription inhibitor actinomycin D was added to MPC5 cells, the half-life of *circ -0,000,953* was over 24 h, while that of linear *R3hcc1l* was about 12 h (Figure S1H).

Overexpression of circ -0,000,953 *alleviated podocyte injury and promoted podocyte autophagy in vitro*

For stable overexpression of *circ -0,000,953*, lentivirus-*circ -0,000,953* (LV-*circ -0,000,953*) was transfected into MPC5 cells, followed by puromycin (1 µg/mL) treatment for 10 days. The transfection efficiency was determined, and *circ -0,000,953* expression was increased approximately 50-fold in MPC5 cells (Figure 2A). The expression of podocyte marker proteins including WT1 and NPHS1/Nephrin can reflect the degree of podocyte injury. Functionally, overexpression of *circ -0,000,953* restored the expression of WT1 and NPHS1 in high glucose (HG)-stimulated cells (Figure 2B). Furthermore,
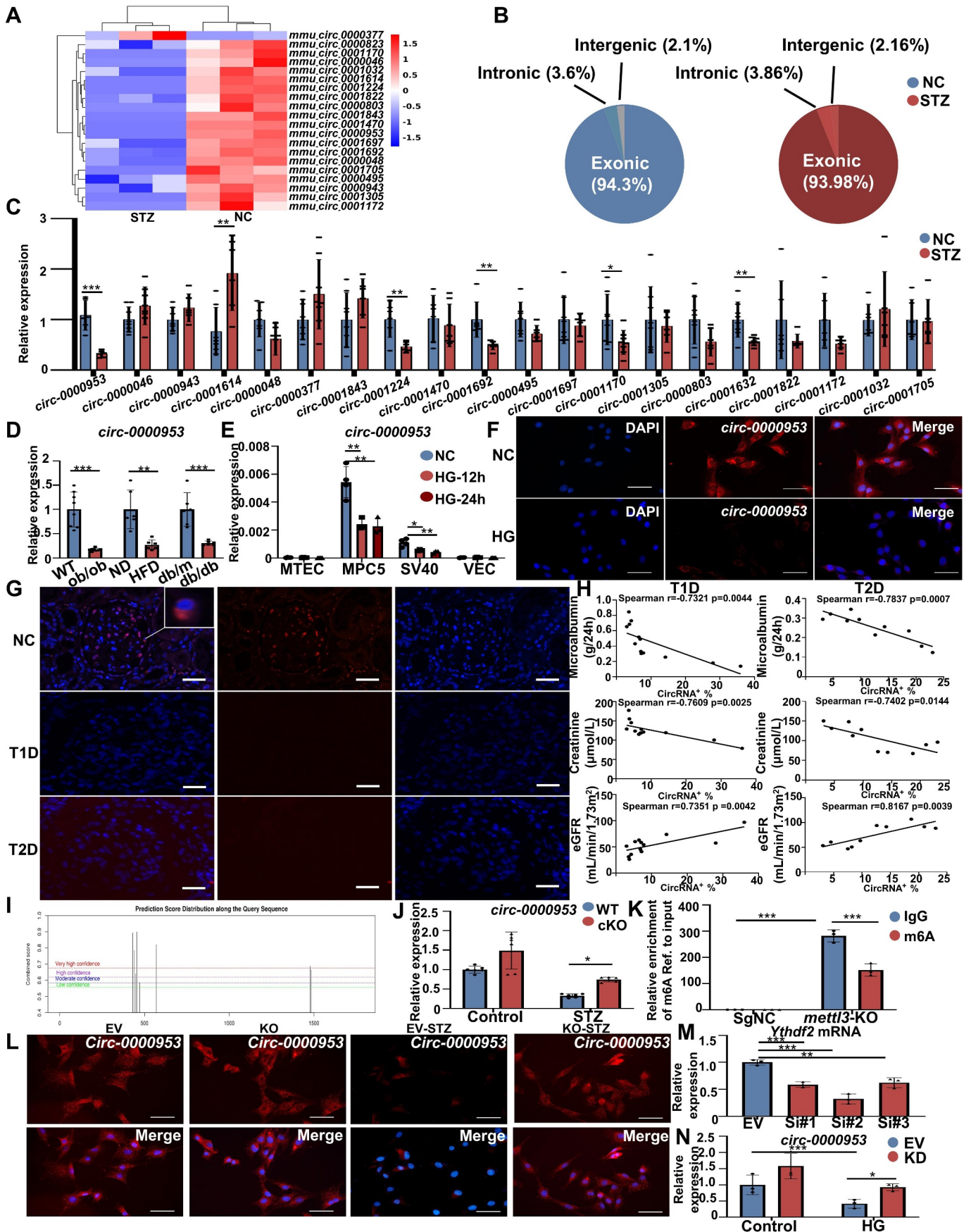
Figure 1. *Circ -0,000,953* was downregulated in DN mice and patients. (A) the heat map reflected the top 20 circRNAs with high homology and the most significant variation. (B) distribution composition of differentially changed circRNAs. (C) the expression level of *circ -0,000,953* in the glomerulus of STZ-induced T1D mice was detected by real-time PCR. (D) *circ -0,000,953* expression level in T2D mice glomerulus was detected by real-time PCR. (E) *circ -0,000,953* expression levels in intrinsic renal cells were detected by real-time PCR. (F) validation of circRNA localization in podocytes by FISH experiments. Scale: 50 μm. (G) FISH experiments demonstrated

real-time PCR revealed that *circ* -0,000,953 overexpressed reduced the inflammatory cytokine *Tnf* and *Il1b* (Figure 2C).

To explore the mechanism by which overexpression of *circ* -0,000,953 reduced podocyte injury, podocytes overexpressing *circ* -0,000,953 were subjected to RNA-seq. Remarkable changes were found in autophagy and PI3K-AKT, a key pathway regulating autophagy (Figure 2D). We further used autophagy inducers (rapamycin) and inhibitors (bafilomycin A$_1$) to investigate the function of *circ* -0,000,953. Results showed that overexpression of *circ* -0,000,953 restored the protein level of ATG7, ATG4B and the accumulation of LCB-II in HG, rapamycin and bafilomycin A$_1$-stimulated cells. Additionally, overexpression of *circ* -0,000,953 inhibited the accumulation of SQSTM1/p62 (Figure 2E). Transmission electron microscopy (TEM) revealed that overexpression of *circ* -0,000,953 significantly increased the number of autophagosomes (AP) and autolysosomes (AL) (Figure 2F). We assessed fusion by double immunostaining for MAP1LC3B/LC3B and the lysosome marker LAMP1 (lysosomal-associated membrane protein 1). There was a significant decrease in the number of LC3B$^+$ LAMP1$^+$ autolysosomes and LC3B$^-$ LAMP1$^+$ autophagosomes in HG-treated podocytes compared to control cells and this effect was reversed by *circ* -0,000,953 overexpression (Figure 2G). We further transfected podocytes with AdmCherry-GFP-LC3B adenovirus to monitor the autophagy flux. Owing to the fact that yellow dots (merged by mCherry and GFP fluorescence) indicated the AP that are not fused with lysosome, while red dots (mCherry fluorescense) indicate the AL that have been fused with lysosome (Figure 2H), both yellow and red dots were increased after overexpression of *circ* -0,000,953.

Podocyte conditional knockin circ -0,000,953 ameliorated renal injury in STZ-induced type 1 diabetic mice

Mice with podocyte conditional knockin (cKI) of *circ* -0,000,953 were generated to prove the function of *circ* -0,000,953 in podocyte injury *in vivo*. In these mice, *circ* -0,000,953 were specifically ablated in podocytes by using the Cre-LoxP recombination system (Figure 3A). *Nphs2*-Cre mice were crossed with *circ* -0,000,953$^{KI/KI}$ mice to generate *Nphs2*-Cre *circ* -0,000,953$^{KI/KI}$ mice, which were identified via tail genotyping (Figure 3B). Real-time PCR was performed to validate the expression of *circ* -0,000,953 in the kidney (Figure 3C). The 24 h urinary ALB (albumin) excretion rate and kidney weight:body weight were markedly decreased in cKI mice (Figure 3D,E). However, *circ* -0,000,953 cKI did not reduce blood glucose levels in diabetic mice (Figure 3F). PAS staining revealed that *circ* -0,000,953 cKI reduced the severity of mesangial dilatation and

tubulointerstitial injury in STZ-induced diabetic mice (Figure 3G). TEM showed that *circ* -0,000,953 cKI significantly alleviated thickening of the renal basement membrane and foot process fusion in STZ-induced diabetic mice (Figure 3H). Additionally, the expression of WT1 and NPHS1 was recovered after *circ* -0,000,953 cKI (Figure 3I–K).

The expressions of ATG7, ATG4B, SQSTM1/p62 and LC3B-II in the kidney tissues of STZ-induced diabetic mice were markedly reversed after *circ* -0,000,953 cKI (Figure 4A). As shown in Figure 4B, *circ* -0,000,953 cKI partially restored the expression of LC3B in the glomerular podocytes of STZ-induced diabetic mice. In Figure 4C, *circ* -0,000,953 cKI suppressed the phosphorylation of RELA/p65. Consistently, *circ* -0,000,953 cKI remarkably reduced the levels of *Tnf* (Figure 4D,E).

Podocyte conditional knockin circ -0,000,953 ameliorated renal injury in HFD-induced type 2 diabetic mice

Real-time PCR was performed to validate the expression of *circ* -0,000,953 in the glomerulus (Figure 5A). The 24 h urinary ALB excretion rate was markedly decreased in cKI mice (Figure 5B). However, *circ* -0,000,953 cKI did not reduce blood glucose levels that were significantly up-regulated in the type 2 DM model (Figure 5C). Further, *circ* -0,000,953 cKI reduced the severity of mesangial dilatation and tubulointerstitial injury and alleviated thickening of the renal basement membrane and foot process fusion in HFD-induced diabetic mice (Figure 5D,E). Additionally, the expressions of WT1 and NPHS1 were recovered after *circ* -0,000,953 cKI (Figure 5F,G). The expressions of ATG7, ATG4B and LC3B-II and the accumulation of SQSTM1/p62 in the glomerulus of HFD-induced diabetic mice were markedly reversed after *circ* -0,000,953 cKI (Figure 5H).

Systemic overexpression of circ -0,000,953 ameliorated renal injury in STZ-induced type 1 diabetic mice

Luciferase-labeled AAV9-*circ* -0,000,953 was injected into the tail vein of mice to establish systemic overexpression of *circ* -0,000,953 mice. Real-time PCR examined the expression of *circ* -0,000,953 in the glomerulus (Figure 6A). At 12 weeks, diabetic mice significantly increased 24 h urinary ALB levels and kidney weight:body weight, which decreased after *circ* -0,000,953 overexpression (Figure 6B,C). However, overexpression of *circ* -0,000,953 did not reduce blood glucose (Figure 6D). PAS staining revealed that *circ* -0,000,953 overexpression reduced the severity of pathological injury (Figure 6E). Also, *circ* -0,000,953 overexpression alleviated

the expression level of *circ* -0,000,953 in renal biopsy specimens and paracancer kidneys of patients with T1D and T2D. Scale: 20 μm. (H) correlation analysis between *circ* -0,000,953 and clinical indexes of diabetic patients. (I) bioinformatics prediction of *circ* -0,000,953 methylation modification sites. (J) the expression level of *circ* -0,000,953 was detected by real-time PCR. (K) the METTL3-mediated m6A modification of *circ* -0,000,953 was detected by MeRIP-qPCR. (L) the expression level of *circ* -0,000,953 was verified by FISH experiment. Scale: 50 μm. (M) the silencing efficiency of *Ythdf2* was verified by real-time PCR. (N) the effect of *Ythdf2* silencing on *circ* -000,953 expression was verified by real-time PCR. Abbreviations: MTEC: mouse renal tubular epithelial cells, MPC5: mouse podocyte cell line; SV40: SV40-MES13-cells, VEC: vascular endothelial cells, NC: normal control, HG: high glucose, EV: empty vector, KD: knockdown, cKO: conditional knockout, STZ: streptozotocin, T1D: type 1 diabetes mellitus, T2D: type 2 diabetes mellitus. *$p < 0.05$, **$p < 0.01$, ***$p < 0.001$.
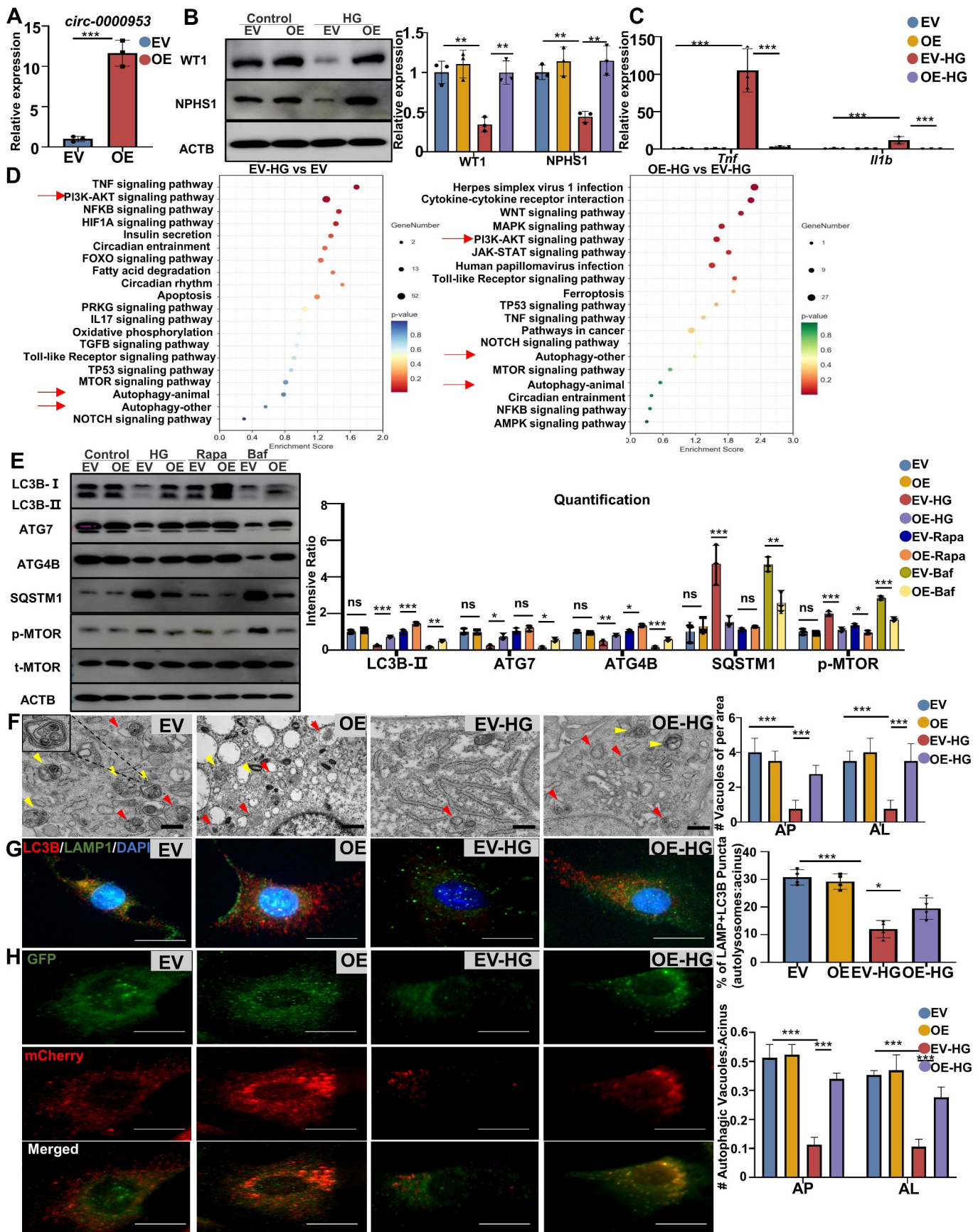
Figure 2. Overexpression of *circ -0,000,953* alleviated podocyte injury and promoted podocyte autophagy *in vitro*. (A) the overexpression effect of *circ -0,000,953* was detected by real-time PCR. (B) Western blot showed that *circ -0,000,953* reversed HG-induced podocyte marker proteins. (C) overexpression of *circ -0,000,953* reduced the expression of inflammatory cytokine *Tnf* and *Il1b* by real-time PCR. (D) KEGG showed that *circ -0,000,953* overexpression regulated signal pathway. (E) Western blot showed that *circ -0,000,953* overexpression regulated key proteins in autophagy. (F) transmission electron microscope (TEM) showed the effect of *circ -0,000,953* overexpression on autophagosome (yellow triangles) and autolysosome (red triangles) in podocytes. Scale: 500 nm. (G) immunofluorescence showed the effect of *circ*

thickening of the renal basement membrane and foot process fusion in T1D mice (Figure 6F). Additionally, *circ -0,000,953* overexpression restored the expression of WT1 and NPHS1 in diabetic mice (Figure 6G-I).

Western blotting showed that *circ -0,000,953* overexpression reversed the changes in the expression of ATG7, ATG4B, LC3B-II and the degradation of SQSTM1/p62 in the glomerulus of diabetic mice (Figure S2A). Immunofluorescence double-staining revealed that *circ -0,000,953* overexpression partially restored the expression of LC3B in the podocytes of diabetic mice (Figure S2B). Instead, overexpression *circ -0,000,953* decreased the expression of *Tnf*, *Il1b* and *Ccl2* and suppressed the phosphorylation of RELA/p65 in diabetic mice (Figure S2C-E).

Systemic overexpression of circ -0,000,953 *significantly ameliorated renal injury in db/db type 2 diabetic mice*

To examine the function of *circ -0,000,953* in db/db mice, *circ -0,000,953* was overexpressed in db/db mice by injecting AAV9-*circ -0,000,953* into tail vein. The expression of *circ -0,000,953* in the kidney of db/db mice at 20 weeks was shown in Figure 7A. The 24 h urinary ALB excretion rate of db/db mice was significantly decreased after overexpression of *circ -0,000,953* (Figure 7B). However, overexpression of *circ -0,000,953* did not reduce the level of blood glucose (Figure 7C). *Circ -0,000,953* overexpression reduced the severity of pathological injury and renal ultrastructure injury in db/db mice (Figure 7D,E). Additionally, *circ -0,000,953* overexpression reversed the content of WT1 and NPHS1 to different degrees (Figure 7F,G). Further, over-expressed of *circ -0,000,953* markedly reversed the changes of ATG7, ATG4B, LC3B-II and SQSTM1/p62 in the glomerulus of db/db mice (Figure 7H).

Knockdown of circ -0,000,953 *aggravated renal injury in both STZ-induced type 1 diabetes and db/db type 2 diabetic mice*

AAV9-sh-*circ -0,000,953* was used to silence *circ -0,000,953* in vivo. Silencing of *circ -0,000,953* aggravated STZ-induced renal injury (Figure 8A) and increased the 24 h urinary ALB excretion rate and kidney weight:body weight but make no difference on blood glucose (Figure 8B–D). PAS staining and TEM revealed that knockdown of *circ -0,000,953* aggravated kidney injury in diabetic mice (Figure 8E-F). Additionally, the reduction of *circ -0,000,953* aggravated the loss of WT1 and NPHS1 to different degrees (Figure 8G–I). Knockdown of *circ -0,000,953* aggravated the decline in ATG7, ATG4B, LC3B-II and increased the accumulation of SQSTM1/p62 in type 1 diabetic mice (Figure S3A,B). And silencing of *circ -0,000,953* promoted the phosphorylation of RELA/p65 in

diabetic mice (Figure S3C). Real-time PCR and immuno-histochemical revealed that knockdown of *circ -0,000,953* promoted the release of *Tnf* (Figure S3D,E).
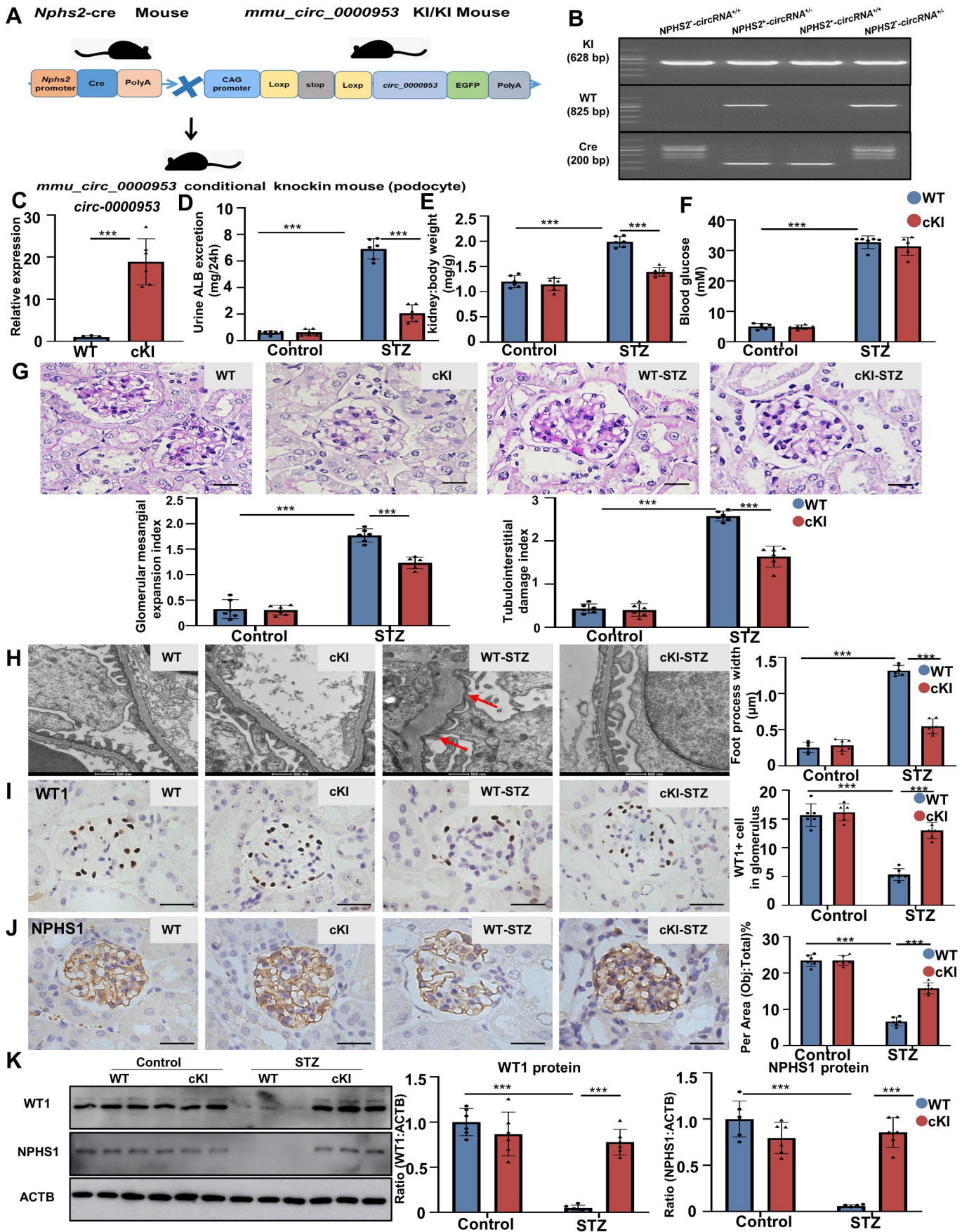
Further, we knockdown *circ -0,000,953* in T2D mice. Real-time PCR validated the expression of *circ -0,000,953* in the kidney (Figure 9A). The 24 h urinary ALB excretion rate were markedly deteriorated in *circ -0,000,953* knockdown mice (Figure 9B). However, *circ -0,000,953* knockdown did not change blood glucose levels (Figure 9C). Further, *circ -0,000,953* knockdown induced the severity of renal pathological injury (Figure 9D,E). The expression of WT1 and NPSH1 was decreased after *circ -0,000,953* knockdown (Figure 9F,G). The level of autophagy in the glomerulus of db/db mice were markedly declined after *circ -0,000,953* knockdown (Figure 9H).

Identification of the interaction between circ -0,000,953-Mir665-3p-Atg4b

CircRNAs can function as miRNA sponges. To identify miRNAs which can bind to *circ -0,000,953* and promising novel miRNAs associated with DN, the interactions between *circ -0,000,953* and its target miRNAs were examined using three public prediction tools, namely, TargetScan, miRanda and RNAhybrid. A Venn diagram was constructed to demonstrate 186 target miRNAs (Figure 10A). Subsequently, TargetScan was used to predict the miRNA targets of human circRNAs homolog with *mmu_circ_0000953*, namely, *hsa_circ_0019390*, and a total of 961 potential target miRNAs were identified (Figure 10A). Further intersection analysis revealed 25 highly conserved miRNAs homolog between humans and mice (Figure 10A). Subsequently, affinity-isolation assay showed that *Mir665-3p* bound to *circ -0,000,953* directly (Figure S4A). The interaction between *circ -0,000,953* and *Mir665-3p* was confirmed by luciferase assay. The Renilla luciferase activity of *circ -0,000,953*-WT was markedly lower in the *Mir665-3p* mimic group than in the negative-control group (Figure 10B). The binding sites of *Mir665-3p* were proved within the *circ -0,000,953* sequence (Figure 10C). FISH assay proved that *circ -0,000,953* and *Mir665-3p* were co-localized in podocytes cytoplasm (Figure 10D).

To identify target genes of *circ -0,000,953*-*Mir665-3p* related to DN, TargetScan was used to predict miRNA target proteins. The *ATG* (autophagy related) gene *Atg4b* was identified as one of the target genes of *Mir665-3p*. The binding sites of *Atg4b* were identified within the *Mir665-3p* sequence (Figure 10E). The Renilla luciferase activity of *Atg4b*-WT was obviously lower in the *Mir665-3p* mimic group than that of negative-control group (Figure 10F).

-0,000,953 overexpression on LC3B with LAMP1 in HG-induced podocytes. Scale: 10 μm. (H) Representative images of MPC5 transfected ad-mCherry-GFP-LC3B adenovirus. Yellow puncta indicated autophagosomes, red puncta indicated autolysosomes. The number of red and yellow LC3 dots per cell were counted. Scale: 10 μm. Abbreviations: EV: empty vector, OE: overexpression, HG: high glucose, Rapa: rapamycin, Baf: bafilomycin A$_1$, AP: autophagosome, AL: autolysosome, ns: no significance. *$p < 0.05$, **$p < 0.01$, ***$p < 0.001$.

Figure 3. Conditional knockin *circ -0,000,953* significantly alleviated kidney injury and podocyte injury in STZ-induced diabetic mice. (A) schematic illustrating the genetic approach used to generate *circ -0,000,953* cKI mice. (B) *circ -0,000,953* cKI was confirmed by assessing genomic DNA. (C) real-time PCR showed the effect of conditional knockin *circ -0,000,953* in glomerulus. (D) mouse urinary ALB ELISA showed that *circ -0,000,953* cKI reduced 24 h urinary ALB excretion rate in STZ-induced diabetic mice. (E) podocytes conditional knockin *circ -0,000,953* reduced kidney weight:body weight of mice. (F) *circ -0,000,953* cKI had no significant effect on blood

Circ -0,000,953 promoted autophagy by targeting Mir665-3p

To assess whether *circ -0,000,953* promotes autophagy by targeting *Mir665-3p*, the *circ -0,000,953* expression and *Mir665-3p* mimic vectors were co-transfected into MPC5 cells cultured in a HG medium. Western blotting found that the *Mir665-3p* mimic aggravated the loss of podocyte-specific marker proteins and abolished the protective effects of *circ -0,000,953* overexpression in MPC5 cells (Figure S5A). Western blot, real-time PCR and immunofluorescence showed that the *Mir665-3p* mimic promoted inflammation and abolished the anti-inflammatory effects of *circ -0,000,953* overexpression in MPC5 cells (Figure S5B–D). Additionally, the *Mir665-3p* mimic significantly aggravated autophagy and abolished the protective effects of *circ -0,000,953* overexpression in MPC5 cells (Figure S5E).

Knockdown of Mir665-3p reduced HG-induced podocyte injury and autophagy disorders in vitro

Mir665-3p was knocked down in MPC5 cells through lentiviral transfection, and the transfection efficiency was validated (Figure 10G). Functionally, *Mir665-3p* knockdown reduced the loss of WT1 and NPSH1 (Figure 10H). Further, knockdown of *Mir665-3p* reduced the content of inflammatory factor and phospho-RELA/p65 NFKB in HG-stimulated cells (Figure 10H,I). Western blotting proved that knockdown of *Mir665-3p* promoted the protein levels of ATG7, LC3B-II and ATG4B, which were downregulated owing to HG treated, and decreased the accumulation of SQSTM1/p62 (Figure 10J).

Knockdown of Mir665-3p alleviated renal injury in STZ-induced type 1 diabetic mice and db/db type 2 diabetic mice

To examine the function of *Mir665-3p*, AAV9-sh-*Mir665-3p* was used to silence *Mir665-3p* (Figure 11A). Silencing of *Mir665-3p* reduced the 24 h urinary ALB excretion rate and kidney weight:body weight but had no change on blood glucose (Figure 11B–D). PAS staining and TEM found that knockdown of *Mir665-3p* alleviated kidney injury in diabetic mice (Figure 11E,F). Additionally, knockdown of *Mir665-3p* alleviated the loss of WT1 and NPSH1 (Figure 11G–11I).

The changes of ATG7, ATG4B, LC3B-II and SQSTM1/p62 were markedly reversed after the knockdown of *Mir665-3p* (Figure S6A). Additionally, immunofluorescence double-staining validated that knockdown of *Mir665-3p* partially promoted the expression of LC3B in the diabetic mouse glomeruli (Figure S6B). Furthermore, knockdown of *Mir665-3p* suppressed the phosphorylation of RELA/p65 in diabetic mice and inhibited the levels of TNF (Figure S6C,D).

Further, we validated the function of *Mir665-3p* in the db/db mice (Figure 12A). The 24 h urinary ALB excretion rate were markedly alleviated in *Mir665-3p* knockdown mice (Figure 12B). However, *Mir665-3p* knockdown did not reduce blood glucose levels in the type 2 DM model (Figure 12C). Further, *Mir665-3p* knockdown reduced the severity of renal pathological injury (Figure 12D,E). Additionally, the expression of WT1 and NPSH1 was restored after *Mir665-3p* knockdown (Figure 12F,G). The level of autophagy in the glomerulus of db/db mice were markedly reversed after *Mir665-3p* knockdown (Figure 12H).

Overexpression of Atg4b alleviated podocyte injury, inflammation and promoted autophagy disorder in vitro

Atg4b was overexpressed in MPC5 cells through plasmid transfection. The result of real-time PCR showed the transfection efficiency of *Atg4b*, and the level of *Atg4b* was increased about 10-fold (Figure 13A). Functionally, overexpression of *Atg4b* restored the expression of WT1 and NPSH1 (Figure 13B,C). Western blotting and real-time PCR indicated that overexpression of *Atg4b* markedly reduced the expression of *Tnf*, *Il1b*, *Ccl2* and phospho-RELA/p65 NFKB in HG-stimulated cells (Figure 13B,D). In addition, overexpression of *Atg4b* recovered the levels of ATG7 and LC3B-II, and inhibited the accumulation of SQSTM1/p62 (Figure 13E). TEM found that overexpression of *Atg4b* increased the number of typical autophagosomes and autolysosomes (Figure 13F). We assessed fusion by double immunostaining for LC3B and LAMP1. There was a significant decrease in the number of LC3$^+$ LAMP1$^+$ autolysosomes and LC3$^-$ LAMP1$^+$ autophagosomes in HG-treated podocytes and this effect was reversed by *Atg4b* overexpression (Figure 13G). We further transfected podocytes with AdmCherry-GFP-LC3B adenovirus to monitor the autophagy flux. As shown in Figure 13H, both yellow (AP) and red dots (AL) increased significantly after overexpression of *Atg4b*.

Overexpression of Atg4b reduced renal injury in mice with STZ-induced type 1 diabetes and db/db type 2 diabetic mice

The effects of *Atg4b* were examined in mice with STZ-induced DN. AAV9-*Atg4b* was injected into the tail vein of mice, and the transfection efficiency was examined using real-time PCR (Figure 14A). Diabetic mice showed remarkable increased 24 h urinary ALB and kidney weight:body weight, which decreased after overexpression of *Atg4b* (Figure 14B,C). Overexpression of *Atg4b* did not change blood glucose in STZ-induced diabetic mice (Figure 14D). PAS staining and TEM revealed that overexpression of *Atg4b* mitigated pathological damage of the kidney in mice with T1D (Figure 14E,F).

---

glucose level. (G) PAS staining showed typical glomerular structural changes in different groups of mice. Scale: 25 μm. (H) the mean thickness of glomerular basement membrane (GBM) and the mean width of foot process of mice were detected by TEM. Scale: 500 nm. (I and J) immunohistochemistry showed that *circ -0,000,953* cKI reversed the content of podocyte makers. Scale: 25 μm. (K) Western blot detected the expression of podocyte marker protein in glomerulus. Abbreviations: WT: wild type, cKI: conditional knockin. ***p < 0.001.
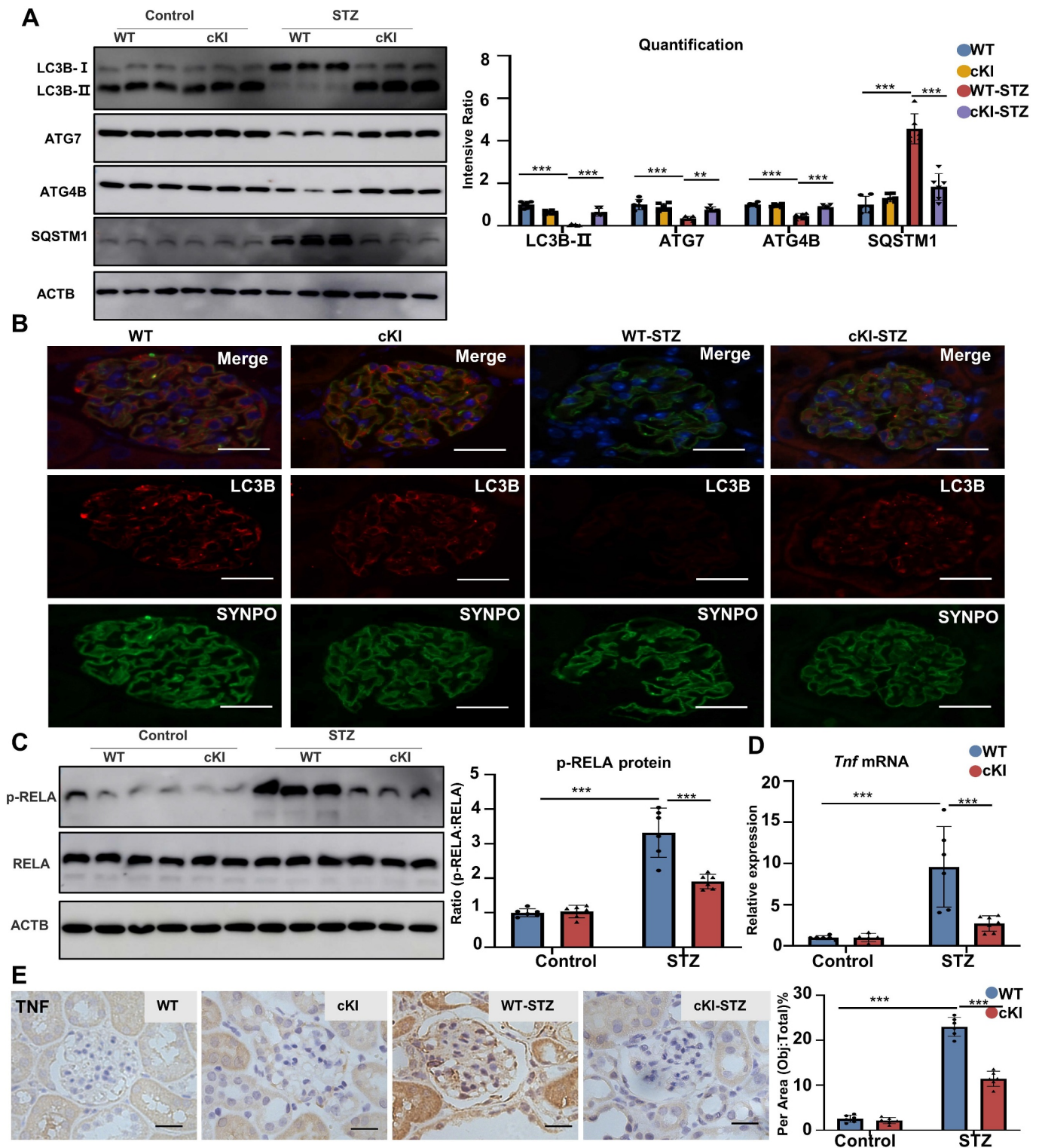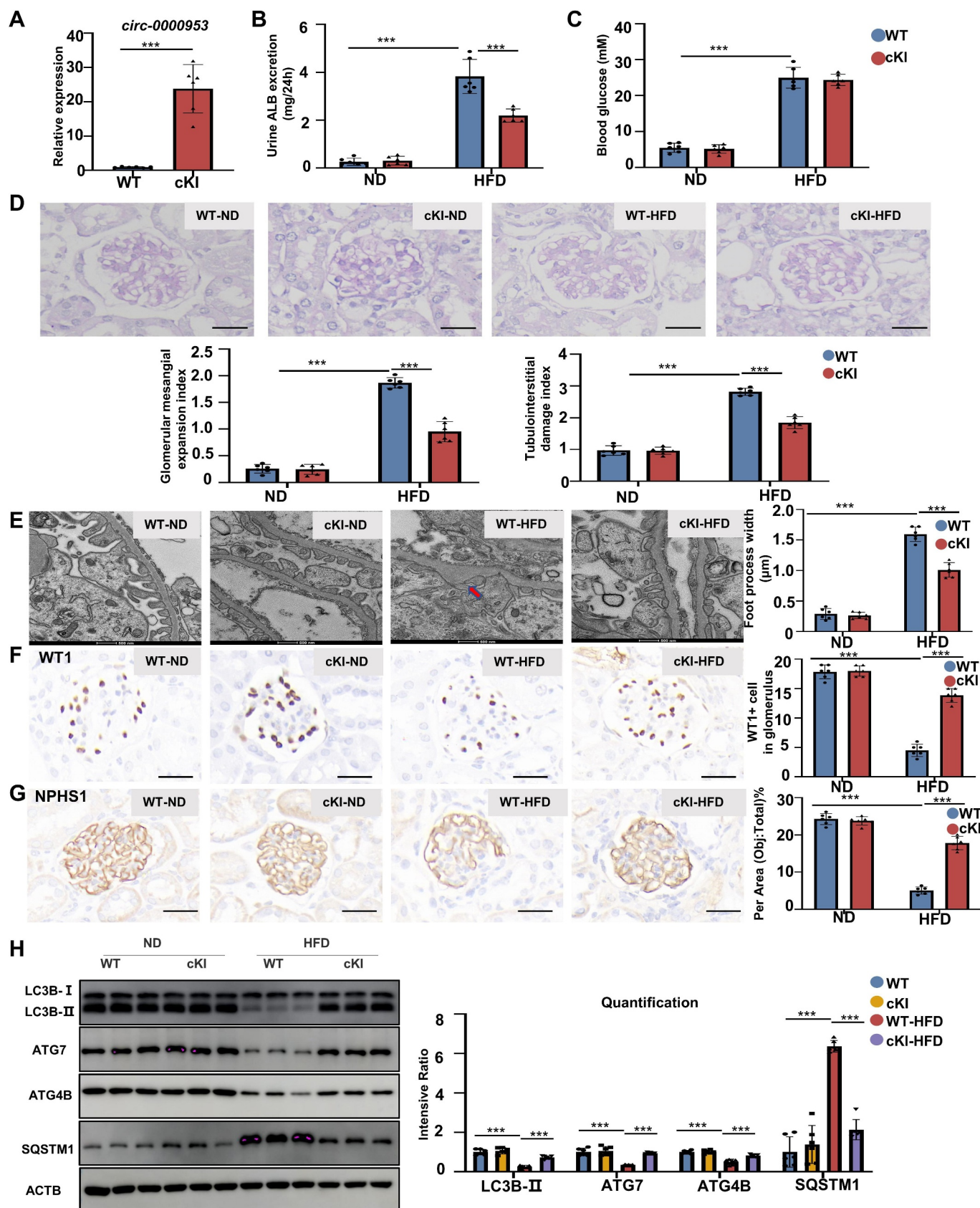
Figure 4. Conditional knockin *circ -0,000,953* of podocyte significantly reduced the autophagy and inflammatory level disorders in STZ-induced type 1 diabetes mice. (A) Western blot showed the expression levels of autophagy related proteins in glomerulus. (B) immunofluorescence showed the expression of autophagy key protein LC3B. Scale: 25 μm. (C) Western blot of RELA/p65 phosphorylation in NFKB pathway. (D) the expression levels of inflammatory factors were detected by real-time PCR. (E) the expression level of inflammatory cytokine TNF was determined by immunohistochemistry. Scale: 25 μm. Abbreviations: WT: wild type, cKI: conditional knockin. **$p < 0.01$, ***$p < 0.001$.

Overexpression of *Atg4b* attenuated the loss of WT1 and NPSH1 in diabetic mice (Figure 14G–I). The changes in the levels of ATG7, LC3B-II and SQSTM1/p62 in diabetic mice kidney were markedly reversed after overexpression of *Atg4b* (Figure S7A,B). In addition, overexpression of *Atg4b* inhibited the phosphorylation of RELA/p65 in mice with T1D and reduced the levels of TNF (Figure S7C – E).

Further, the function of *Atg4b* were examined in T2D mice (Figure 15A). The 24 h urinary ALB excretion rate were markedly decreased in *Atg4b* overexpressed mice

Figure 5. Podocyte conditional knockin *circ -0,000,953* ameliorated renal injury in HFD-induced type 2 diabetic mice. (A) real-time PCR was performed to validate the expression of *circ -0,000,953* in the glomerulus. (B) the 24 h urinary ALB excretion rate was markedly decreased in cKI mice. (C) *circ -0,000,953* cKI did not reduce blood glucose levels in the type 2 DM model. (D) PAS staining showed typical glomerular structural changes in different groups of mice. Scale: 25 μm. (E) the mean thickness of GBM and the mean width of foot process of mice were analyzed by TEM. Scale bar: 500 nm. (F and G) immunohistochemistry showed the expression of WT1 and NPHS1. Scale: 25 μm. (H) Western blot detected the expressions of ATG7, ATG4B, SQSTM1/p62 and LC3B-II in the kidney tissues. Abbreviations: WT: wild type, cKI: conditional knockin, HFD: high-fat diet. **$p < 0.01$, ***$p < 0.001$.
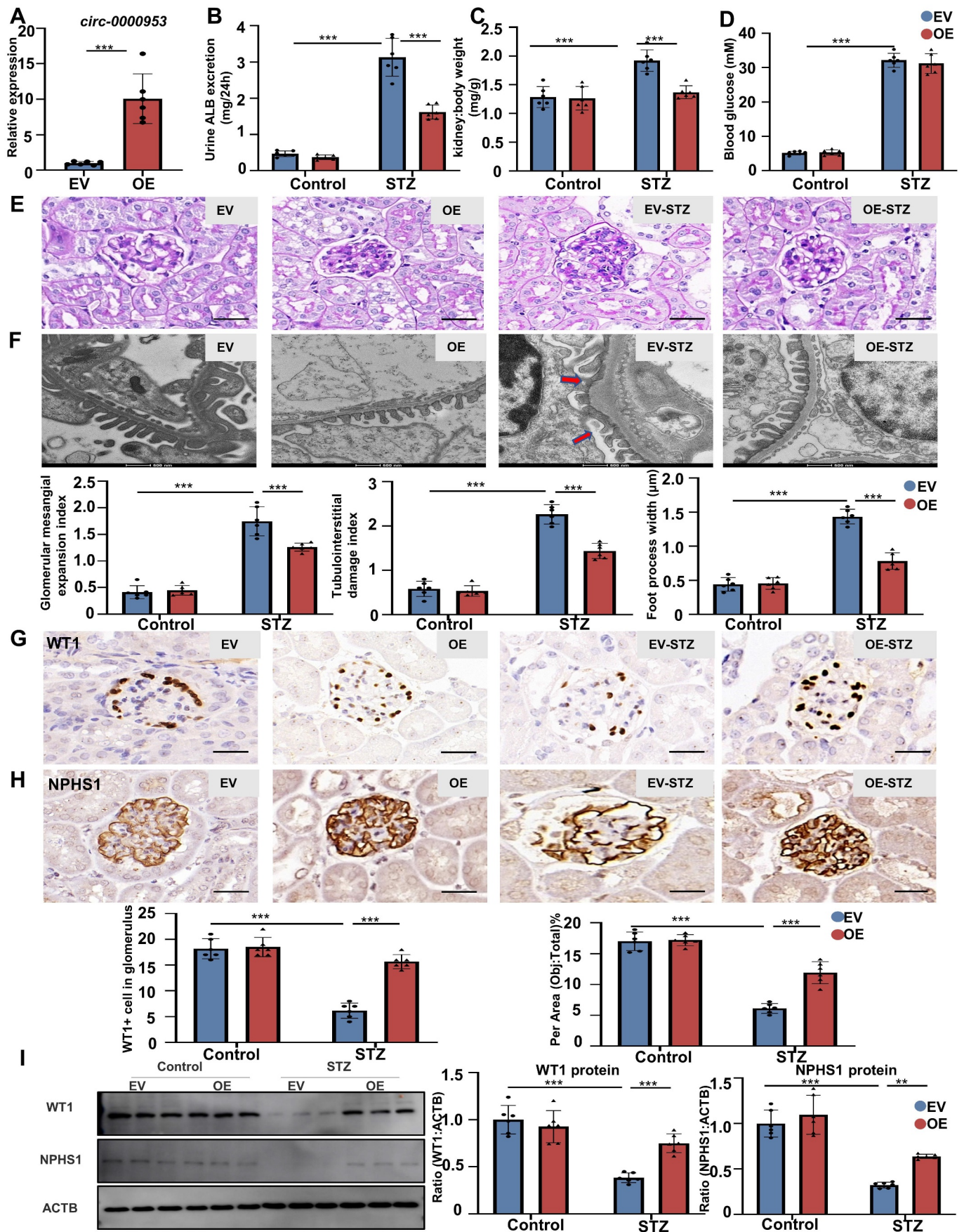
Figure 6. Systemic overexpression of *circ -0,000,953* ameliorated renal injury in STZ-induced type 1 diabetic mice. (A) real-time PCR showed the efficiency of overexpression *circ -0,000,953* in the kidney. (B) *circ -0,000,953* overexpression reduced the 24 h urinary ALB excretion rate of STZ-induced diabetic mice. (C) overexpression of *circ -0,000,953* reduced kidney weight:body weight of mice. (D) overexpression of *circ -0,000,953* had no significant effect on blood glucose. (E) PAS staining showed typical glomerular structural changes in different groups of mice. Scale: 25 μm. (F) the mean thickness of GBM and the mean width of foot process of mice were analyzed by TEM. Scale: 500 nm. (G and H) immunohistochemistry showed that *circ -0,000,953* reversed the expression of WT1 and NPHS1. Scale: 25 μm. (I) Western blot of glomerulus showed the expression level of podocyte marker. Abbreviations: EV: empty vector, OE: overexpression. **$p < 0.01$, ***$p < 0.001$.
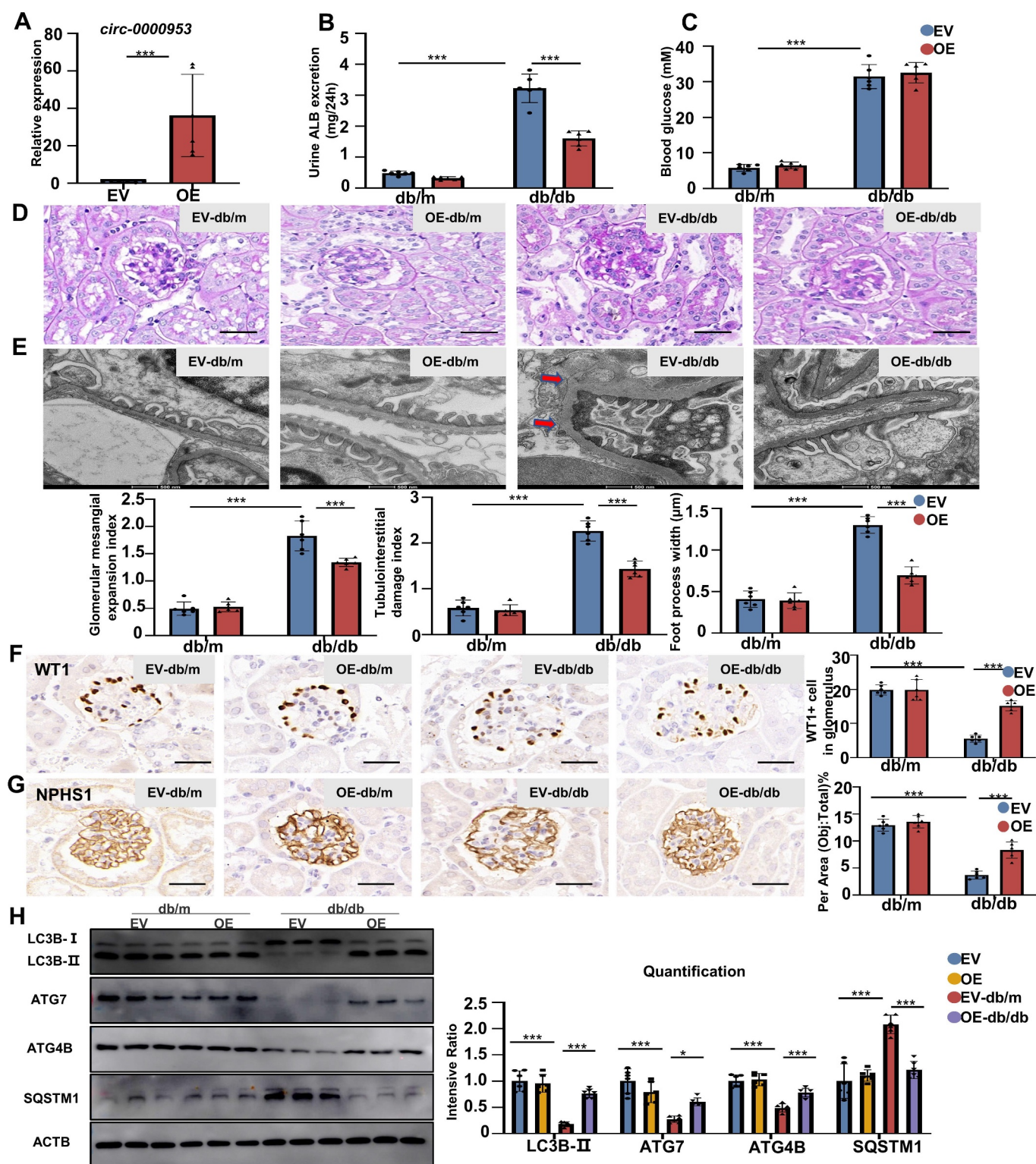
Figure 7. Systemic overexpression of *circ -0,000,953* significantly ameliorated renal injury in db/db type 2 diabetic mice. (A) real-time PCR showed the efficiency of *circ -0,000,953* overexpression in kidney. (B) *circ -0,000,953* overexpression could significantly reduce the 24 h urinary ALB excretion rate of db/db type 2 diabetic mice. (C) overexpression of *circ -0,000,953* had no significant effect on blood glucose. (D) PAS staining showed typical glomerular structural changes in different groups of mice. Scale: 25 μm. (E) the mean thickness of GBM and the mean width of foot process of mice were measured by TEM. Scale: 500 nm. (F and G) immunohistochemistry showed that *circ -0,000,953* reversed the expression of WT1 and NPHS1. Scale: 25 μm. (H) Western blot showed the expression of autophagy related proteins in glomerulus. Abbreviations: EV: empty vector, OE: overexpression. *$p < 0.05$, ***$p < 0.001$.
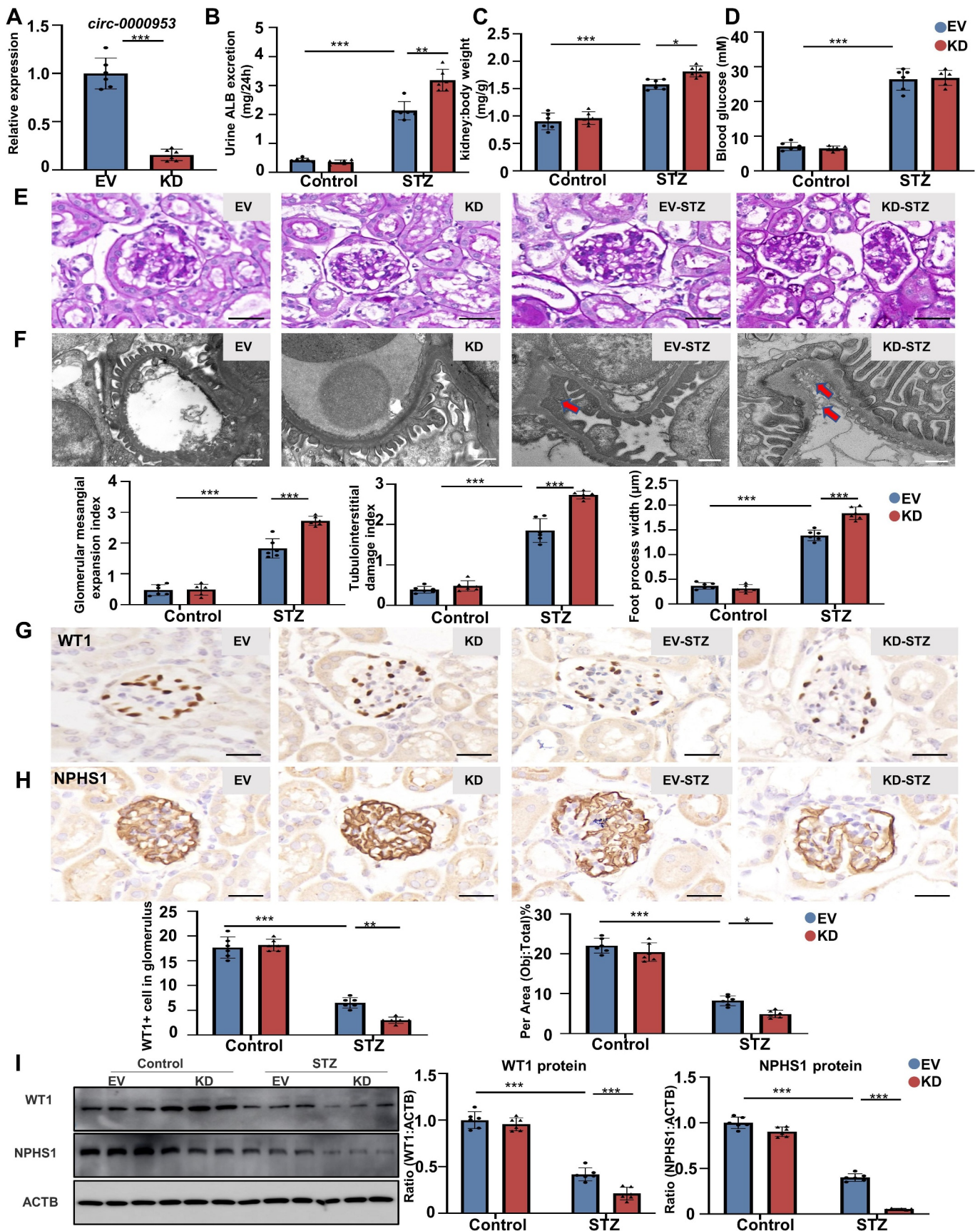
Figure 8. Silencing *circ -0,000,953* aggravated kidney injury and podocyte injury in STZ-induced type 1 diabetes mice. (A) real-time PCR validated the silencing efficiency of *circ -0,000,953*. (B) silencing *circ -0,000,953* could decrease the 24 h urinary ALB excretion rate of STZ-induced diabetic mice. (C) silencing *circ -0,000,953* increased the kidney weight:body weight of mice. (D) silencing *circ -0,000,953* had no significant effect on blood glucose. (E) PAS staining showed typical glomerular structural changes in different groups of mice. Scale: 25 μm. (F) the mean thickness of GBM and the mean width of foot process of mice were detected by TEM. Scale: 500 nm. (G and H) immunohistochemistry showed that silencing *circ -0,000,953* deteriorated the loss of WT1 and NPHS1. Scale: 25 μm. (I) Western blot detected the expression of podocyte marker. Abbreviation: EV: empty vector, KD: knockdown. $*p < 0.05$, $**p < 0.01$, $***p < 0.001$.
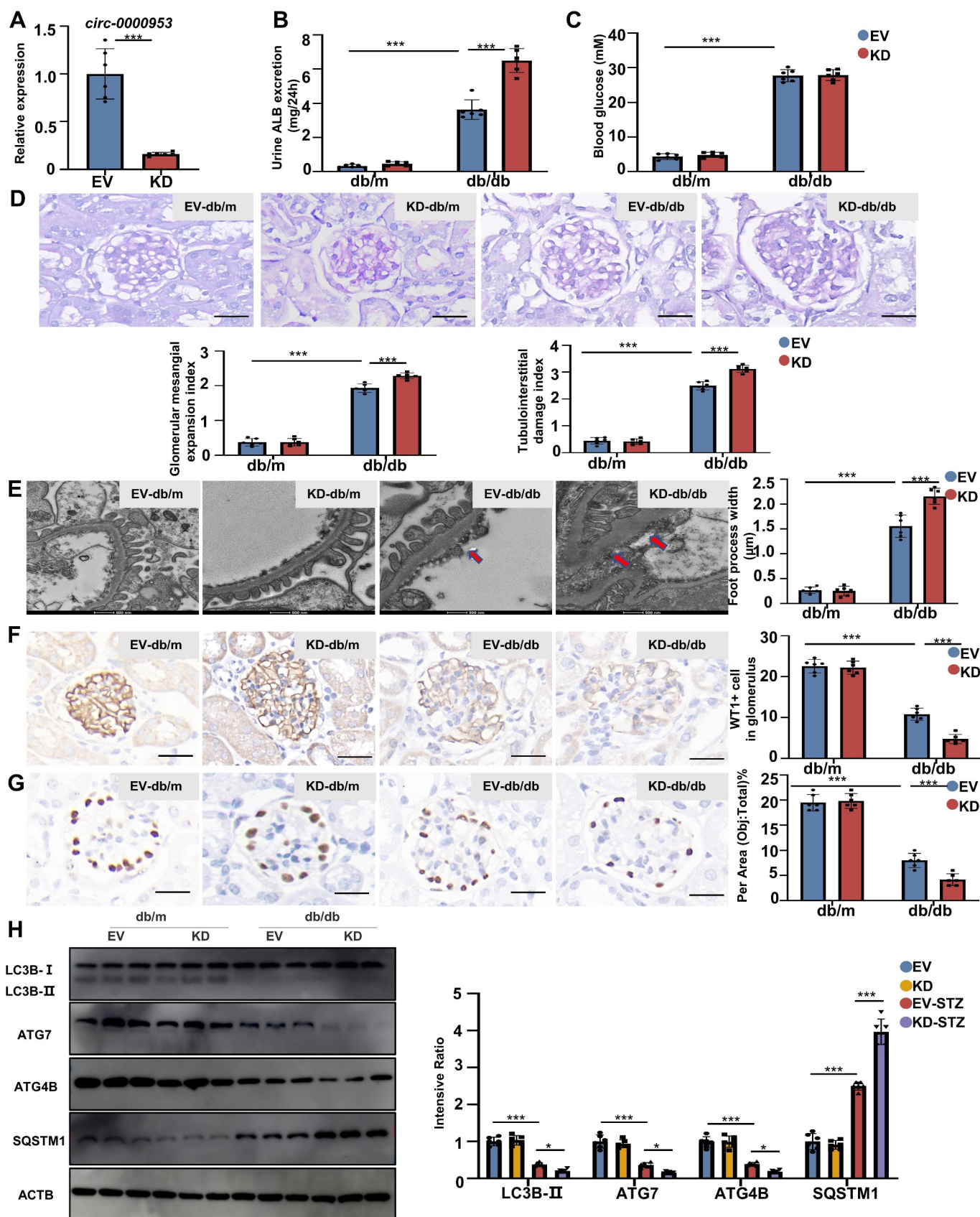
Figure 9. Silencing *circ -0,000,953* significantly aggravated renal injury in db/db mice. (A) real-time PCR validated the silencing efficiency of *circ -0,000,953*. (B) silencing *circ -0,000,953* decreased the 24 h urinary ALB excretion rate of db/db mice. (C) knockdown of *circ -0,000,953* had no significant effect on blood glucose level. (D) PAS staining showed typical glomerular structural changes in different groups of mice. Scale: 25 μm. (E) the mean thickness of GBM and the mean width of foot process of mice were measured by TEM. Scale: 500 nm. (F and G) immunohistochemistry showed the expression of WT1 and NPHS1. Scale: 25 μm. (H) Western blot showed the expression levels of autophagy related proteins in the kidney. Abbreviation: EV: empty vector, KD: knockdown. *p < 0.05, ***p < 0.001.
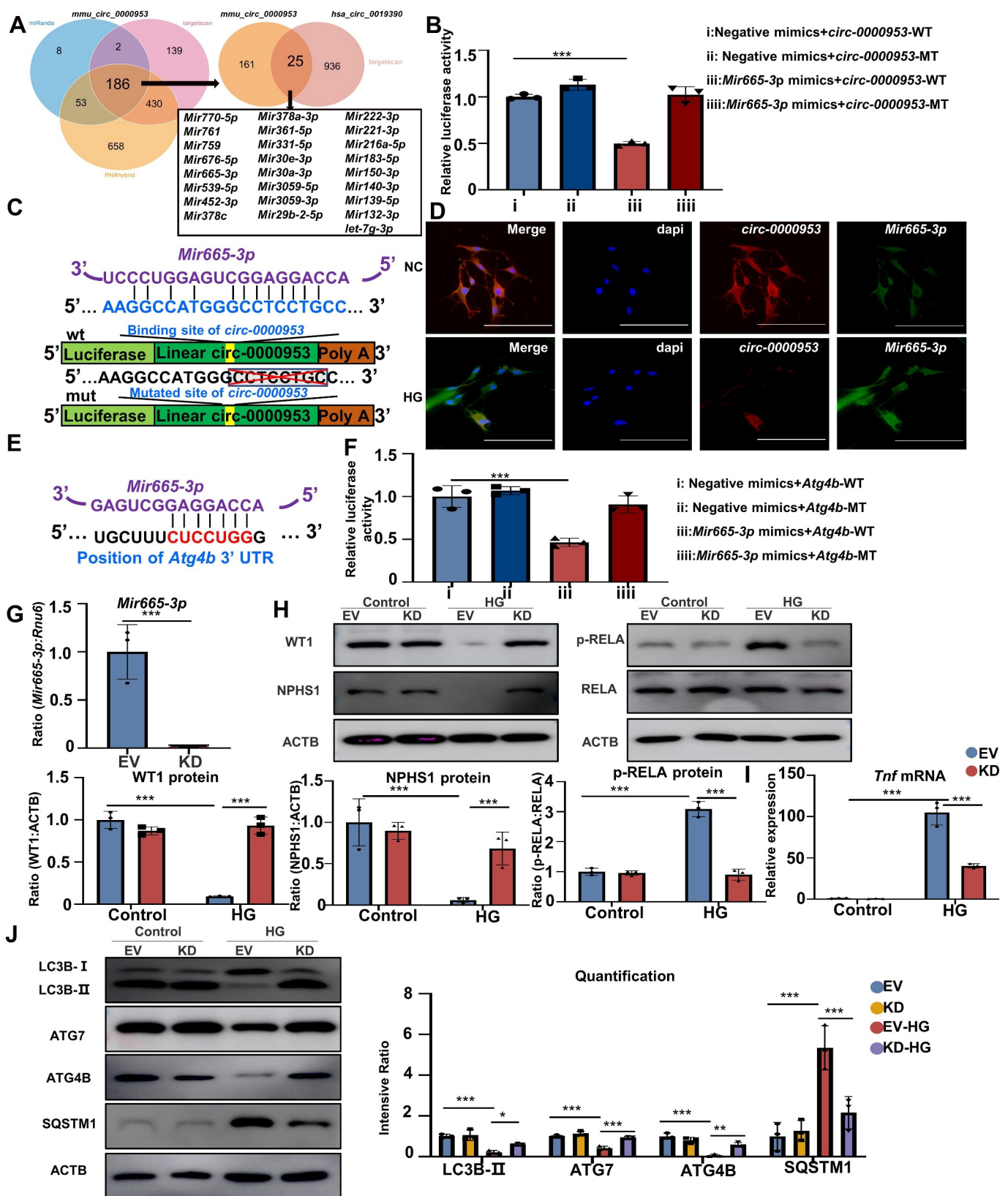
Figure 10. Identification of the interaction between *circ -0,000,953-Mir665-3p-Atg4b*. (A) venn diagram showing the intersection analysis of public prediction sites for *circ -0,000,953* targeted miRNAs. (B) dual luciferase assay demonstrated the interaction of *circ -0,000,953* with *Mir665-3p*. (C) *circ -0,000,953* sequence binding site of *Mir665-3p*. (D) FISH experiments demonstrated that *circ -0,000,953* co-localized with *Mir665-3p* in the cytoplasm of podocytes. Scale: 100 μm. (E) binding site of *Mir665-3p* to *Atg4b*. (F) luciferase reports demonstrate that *Mir665-3p* interacts with *Atg4b*. (G) real-time PCR detected the effect of silencing *Mir665-3p*. (H) Western blot showed that silencing *Mir665-3p* reversed the loss of WT1 and NPHS1, and reduced the phosphorylation of RELA/p65. (I) the effect of silencing *Mir665-3p* on inflammatory factors were detected by real-time PCR. (J) Western blot showed the regulation of silenced *Mir665-3p* on key proteins of autophagy. Abbreviation: EV: empty vector, KD: knockdown, HG: high glucose. $*p < 0.05$, $**p < 0.01$, $***p < 0.001$.
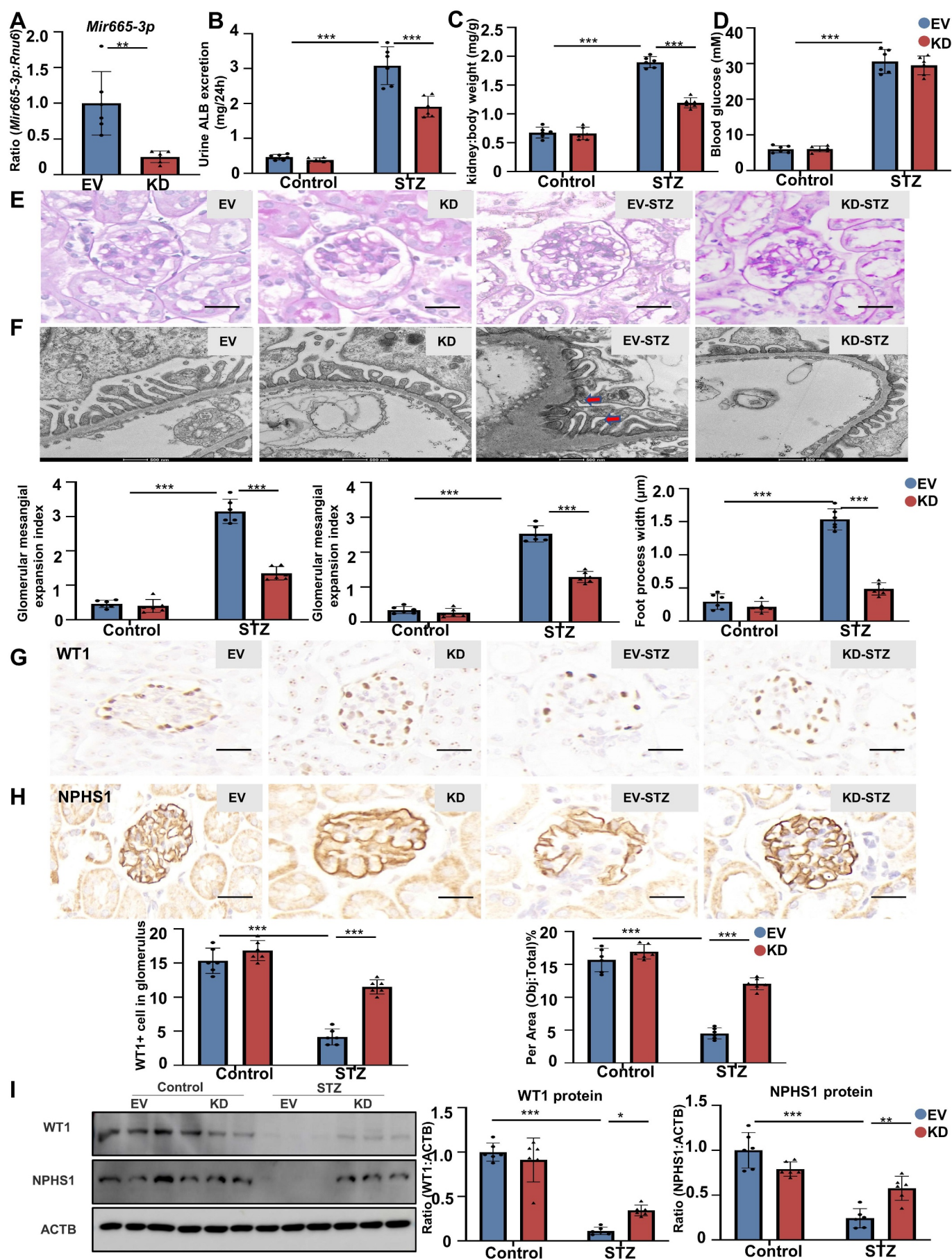
Figure 11. Silencing *Mir665-3p* mitigated kidney damage in STZ-induced diabetic mice. (A) real-time PCR showed the effect of *Mir665-3p* silencing in the kidney. (B) silencing *Mir665-3p* reduced the 24 h urinary ALB excretion rate of STZ-induced diabetic mice. (C) *Mir665-3p* silencing reduced kidney weight:body weight of mice. (D) *Mir665-3p* silencing had no significant effect on blood glucose level. (E) PAS staining showed typical glomerular structural changes in different groups of mice.

(Figure 15B). However, *Atg4b* overexpressed did not reduce blood glucose levels (Figure 15C). Further, overexpression of *Atg4b* reduced the severity of renal pathological injury (Figure 15D,E). Additionally, the expression of WT1 and NPSH1 was restored after *Atg4b* overexpressed (Figure 15F, G). The level of autophagy in the glomerulus of db/db mice were markedly upregulated after *Atg4b* overexpressed (Figure 15H).

Discussion

CircRNA is a popular target for the treatment of human diseases [25–27]. In this study, the expression of *circ -0,000,953* was downregulated both in the kidneys of diabetic mice, HG-induced podocytes and the renal biopsy samples of patients with DN. Furthermore, overexpression of *circ -0,000,953* and podocytes conditional knockin of *circ -0,000,953* ameliorated the progression of T1D and T2D mice and restored podocyte autophagy. Mechanistically, *circ -0,000,953* inhibited the progression of DN by sponging *Mir665-3p* to promote the expression of *Atg4b*. Additionally, m6A methylation enzymes METTL3 was proved to regulate the expression and methylation level of *circ -0,000,953*. Altogether, this study suggested that *circ -0,000,953* deficiency exacerbated podocyte injury and autophagy disorder by targeting *Mir665-3p-Atg4b* in DN. Therefore, *circ -0,000,953* is a potential biomarker for the prophylaxis and treatment of DN.
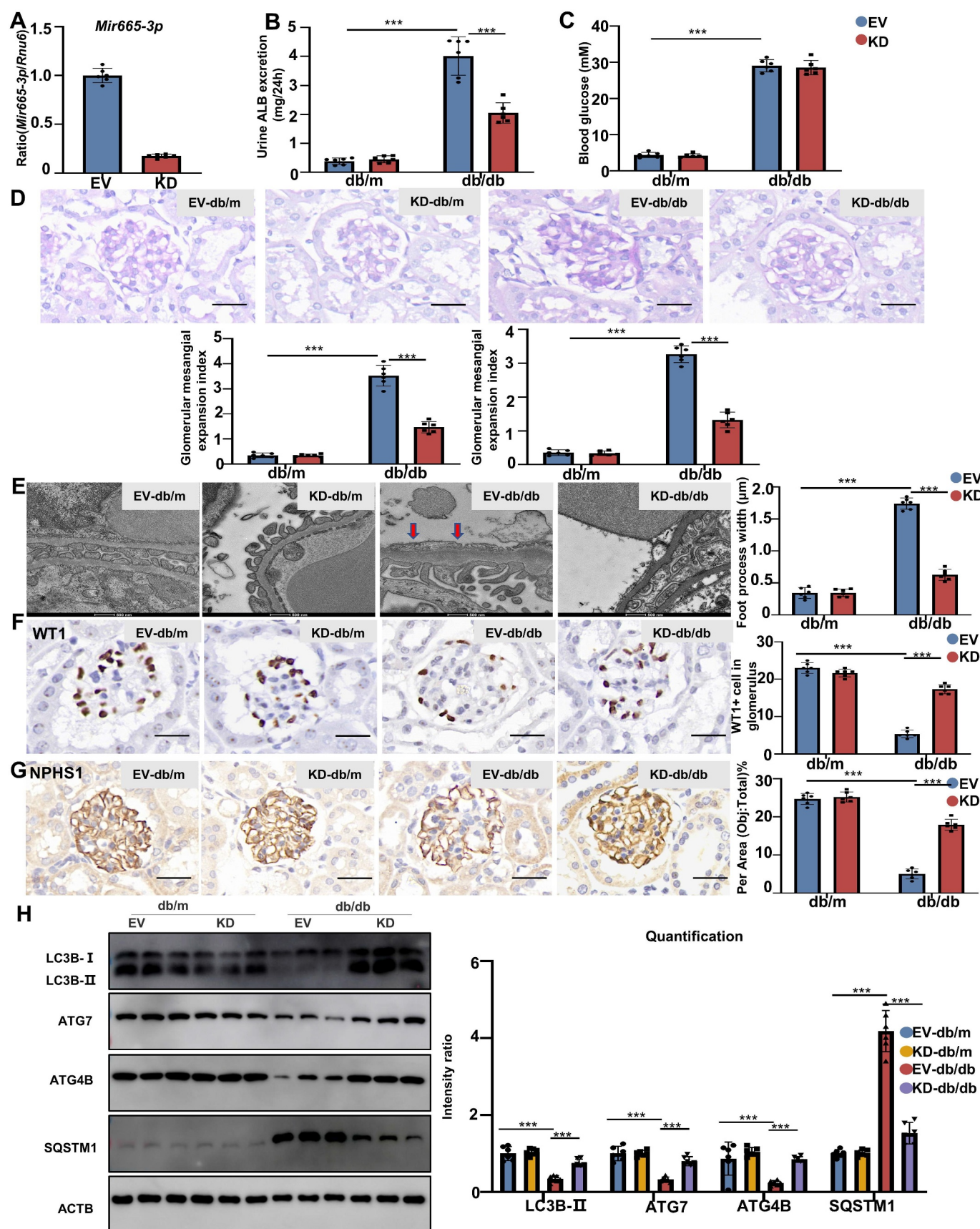
In our research, podocyte-specific *circ -0,000,953* was found to play a role in DN. Compared with the role of miRNAs and lncRNAs, that of circRNAs in injury and repair of kidney has been examined in a limited number of studies [22]. Cheng et al. demonstrated that many circRNAs were expressed differently in rat kidneys with hypertensive nephropathy [26]. Luan et al. reported that *circHLA-C-miR-150* axis plays a pivotal role in lupus nephritis [27]. The *circRNA ZNF609* can promote the expression of *FOXP4* by sponging *Mir138-5p* in renal carcinoma [28]. Additionally, *ciRs-126* expression is high in the peripheral blood of AKI patients [29]. Recent research has reported that circRNAs play regulative function in DN. The *circRNA LRP6* can mediate HG-induced ECM accumulation in mouse mesangial cells by sponging *Mir205* [30]. *CircRNA_010383* inhibits ECM synthesis by promoting the expression of *TPRC1* and *E-cadherin* in MTECs [31]. Despite evidence of changes in circRNAs expression in DN, direct evidence for the role of circRNAs in DN podocytes injury remains lacking. This study was first to revealed that *circ -0,000,953* regulated podocyte injury and autophagy in DN.

Podocyte injury is involved in autophagy dysfunction, and autophagy levels in the kidney are inhibited in the early stages of diabetes [2–4]. This study revealed that systemic overexpression or *circ -0,000,953* cKI in podocytes alleviated diabetes-induced dysfunction of autophagy in mice. So far, this study was the first to show that overexpression of *circ -0,000,953* promotes autophagy in diabetic mice. Autophagy is a process of phagocytosis of cytoplasmic proteins or organelles and fusion with lysosomes to form autophagy lysosomes and degrade the contents contained in them [32]. Autophagy can meet the metabolic needs of cells and renew some organelles [33]. The important role of autophagy in the maintenance of renal function has been elucidated in specific autophagy deficient mice [34]. Moreover, autophagy is involved in podocyte maturation, which is regulated by the Notch pathway [35]. The autophagic process involves a group of *ATG* genes that are conserved from yeast to humans [36]. ATG-mediated autophagy plays a crucial role in the control of inflammatory and apoptotic signaling. As a novel cysteine protease, Atg4b exerts its function as both a processing and a deconjugating protease in the efficient progression of autophagy [36]. In this study, we found *circ -0,000,953* regulated podocyte autophagy by targeting *Mir665-3p-Atg4b* in DN.

Circ -0,000,953 was found to exert anti-inflammatory effects on HG-stimulated cells and diabetic mice. Metabolic, biochemical, and hemodynamic disturbances in DN can activate inflammatory responses [37,38]. In the early stage of DN, the glomeruli and interstitium of the kidney will attack with macrophage and T cell, activated macrophages release many pro-inflammatory, pro-fibrotic and anti-vascular endothelial growth factors [39]. There is also growing evidence that autophagy is involved in maintaining the balance of inflammatory responses after elimination of invading pathogens. Defects in autophagy can lead to excessive inflammation Specific inhibition of inflammatory signaling pathway can alleviate kidney injury in DN mice, thus alleviating DN progression [40]. In this study, we firstly found that overexpression *circ -0,000,953* can reduce inflammation in DN.

CircRNAs, contain multiple miRNA binding sites or miRNA response elements, act as miRNA sponges. Based on miRNA-mediated mRNA cleavage, circRNAs substantially regulate target gene expression. To identify miRNAs that can bind to *circ -0,000,953* and promising novel miRNAs associated with DN, the interactions between *circ -0,000,953* and its target miRNAs were examined using the public prediction tools. We verified that *circ -0,000,953* sponging *Mir665-3p* and the effects of *circ -0,000,953* on DN were partially abrogated after enhancing *Mir665-3p* levels. Additionally, we proved that *Mir665-3p* binds to the 3'UTR of *Atg4b*. Mechanistically, *circ -0,000,953* affects autophagy and inflammation may be related to *Mir665-3p* and its target gene, *Atg4b*. Studies on *Mir665-3p* have shown that it controls multiple functional targets, including *TREM2*, *SDC1* (syndecan 1) and *SMAD3* [41–43]. *Mir665-3p-Atg4b*-autophagy axis relieves inflammation and apoptosis in intestinal ischemia/reperfusion. Inhibition of *Mir665-3p* enhances autophagy and alleviates inflammation in *Fusarium solani*-induced keratitis [44]. Collectively, this study revealed a novel regulatory axis formed by *circ -0,000,953- Mir665-3p- Atg4b* in DN.
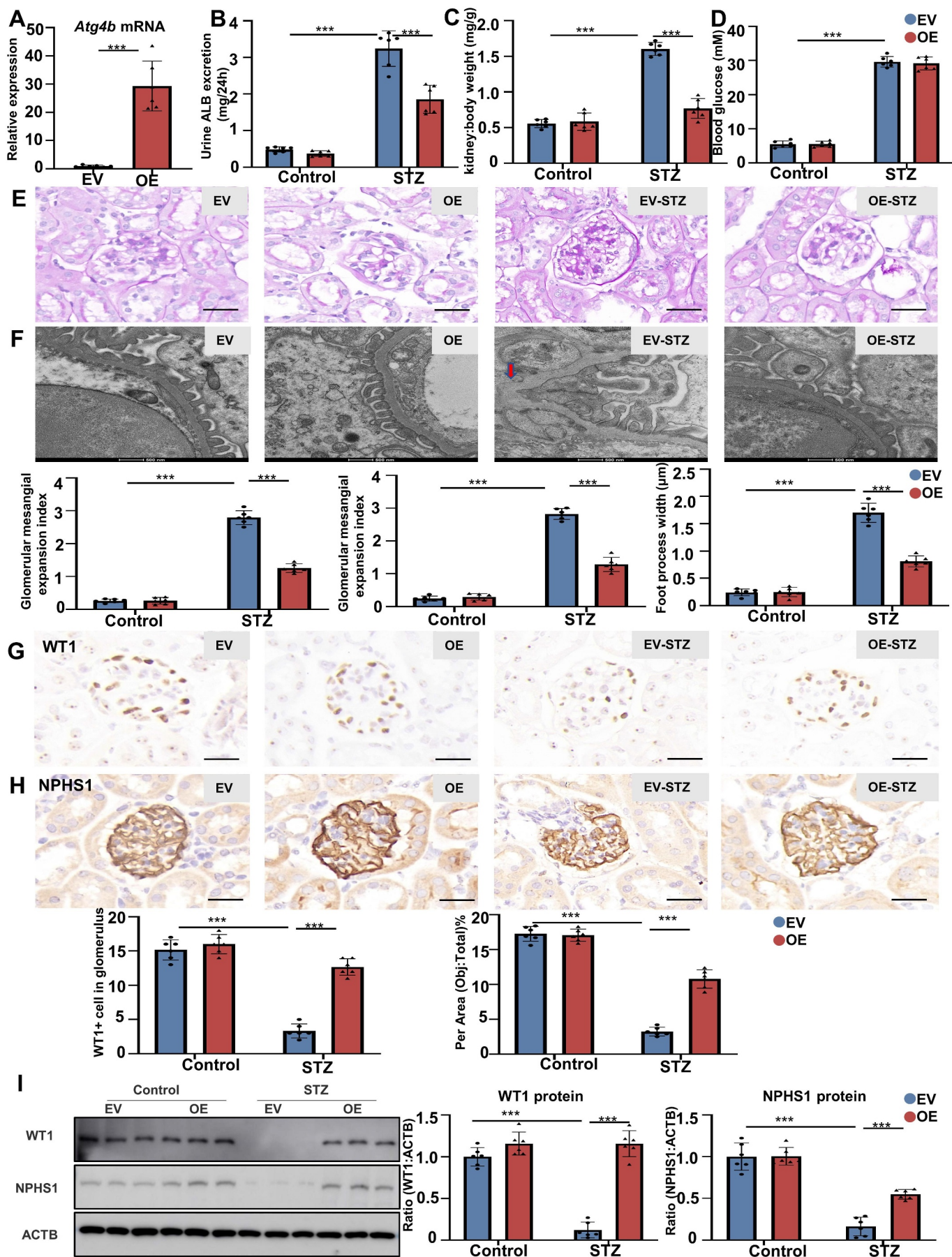

Scale: 25 μm. (F) the mean thickness of GBM and the mean width of foot process of mice were detected by TEM. Scale: 500 nm. (G and H) immunohistochemistry showed that *Mir665-3p* silencing reversed the expression of WT1 and NPHS1. Scale: 25 μm. (I) Western blot detected the expression of podocyte marker protein in glomerulus. Abbreviation: EV: empty vector, KD: knockdown. *$p < 0.05$, **$p < 0.01$, ***$p < 0.001$.

Figure 12. Silencing *Mir665-3p* mitigated kidney damage in db/db type 2 diabetic mice. (A) real-time PCR validated the silencing efficiency of *Mir665-3p*. (B) silencing *Mir665-3p* could reverse the 24 h urinary ALB excretion rate of db/db mice. (C) knockdown of *Mir665-3p* had no significant effect on blood glucose level. (D) PAS staining showed typical glomerular structural changes in different groups of mice. Scale: 25 μm. (E) the mean thickness of GBM and the mean width of foot process of mice were measured by TEM. Scale: 500 nm. (F and G) immunohistochemistry showed the expression of WT1 and NPHS1. Scale: 25 μm. (H) Western blot showed the expression of autophagy related proteins in the kidney. Abbreviation: EV: empty vector, KD: knockdown. *$p < 0.05$, **$p < 0.01$, ***$p < 0.001$.
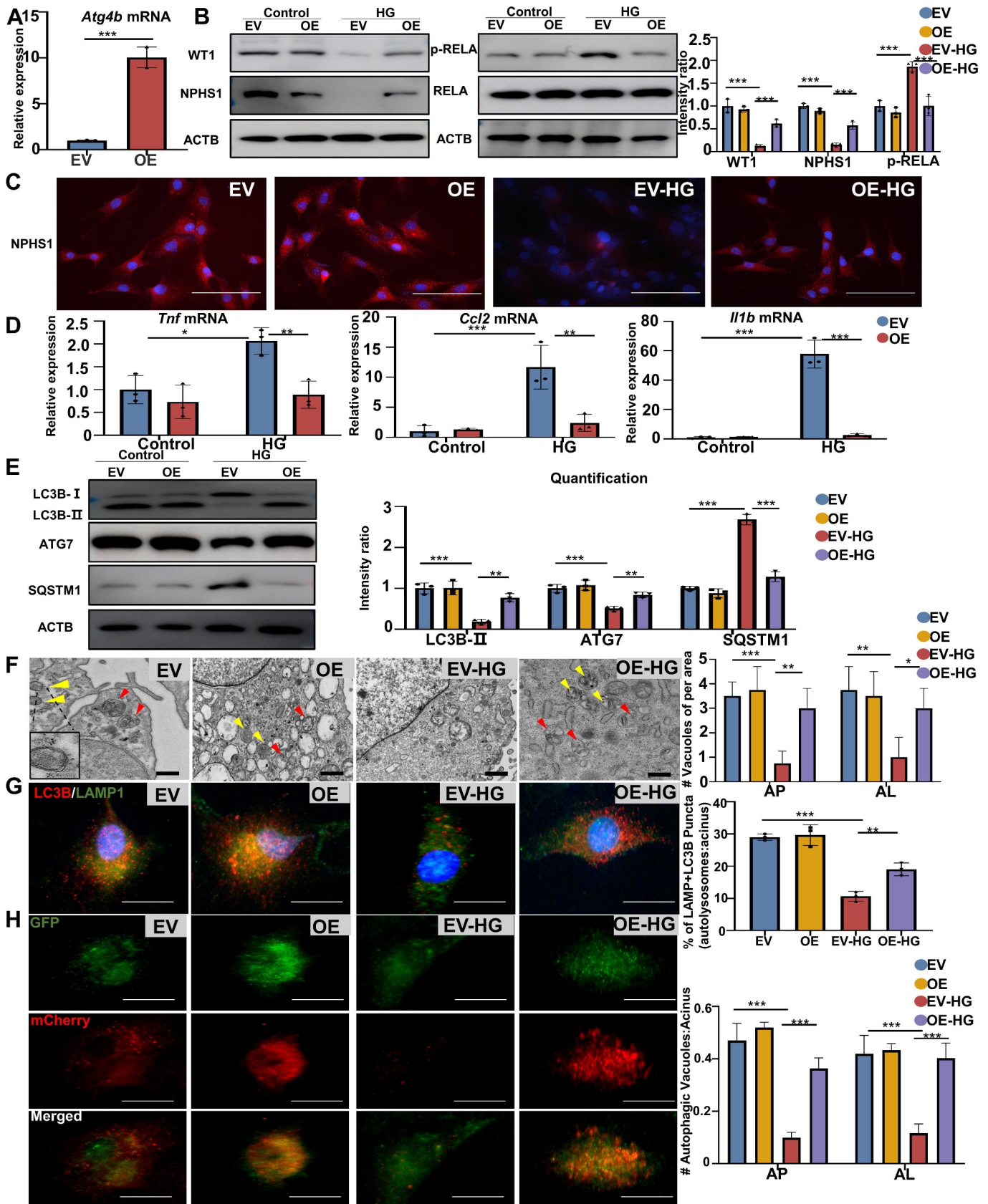
Figure 13. Overexpression of *Atg4b* significantly reduced HG-induced podocytes injury. (A) the efficiency of *Atg4b* overexpression was detected by real-time PCR. (B) Western blot showed that overexpression of *Atg4b* reversed the loss of WT1 and NPHS1, and reduced the phosphorylation of RELA/p65. (C) overexpression of *Atg4b* reversed the loss of HG-induced podocyte marker by immunofluorescence. Scale: 100 μm. (D) real-time PCR confirmed that overexpression of *Atg4b* reduced the expression of inflammatory cytokines. (E) Western blot showed the regulation of key autophagy proteins by overexpression of *Atg4b*. (F) TEM showed the effect of *Atg4b* overexpression on autophagosome and autolysosome in podocytes. Scale: 500 nm. (G) immunofluorescence showed the effect of *Atg4b* overexpression on LC3B with LAMP1 in HG-induced podocytes. Scale: 10 μm. (H) Representative images of MPC5 transfected ad-mCherry-GFP-LC3B adenovirus. Yellow puncta indicated autophagosomes, red puncta indicated autolysosomes. Scale: 10 μm. Abbreviation: EV: empty vector, OE: overexpression, HG: high glucose. *$p < 0.05$, **$p < 0.01$, ***$p < 0.001$.

Figure 14. Overexpression of *Atg4b* mitigated kidney damage in STZ-induced diabetic mice. (A) real-time PCR showed the efficiency of overexpression *Atg4b* in the kidney. (B) overexpression of *Atg4b* reduced the 24 h urinary ALB excretion rate of STZ-induced diabetic mice. (C) overexpression of *Atg4b* reduced kidney weight: body weight of mice. (D) *Atg4b* overexpression had no significant effect on blood glucose. (E) PAS staining showed typical glomerular structural changes in different groups of mice. Scale: 25 μm. (F) the mean thickness of GBM and the mean width of foot process were analyzed by TEM. Scale: 500 nm. (G and H) immunohistochemistry showed that overexpression of *Atg4b* reversed the expression of podocyte markers. Scale: 25 μm. (I) Western blot detected the expression of podocyte marker protein in glomerulus. Abbreviation: EV: empty vector, OE: overexpression. ***$p < 0.001$.
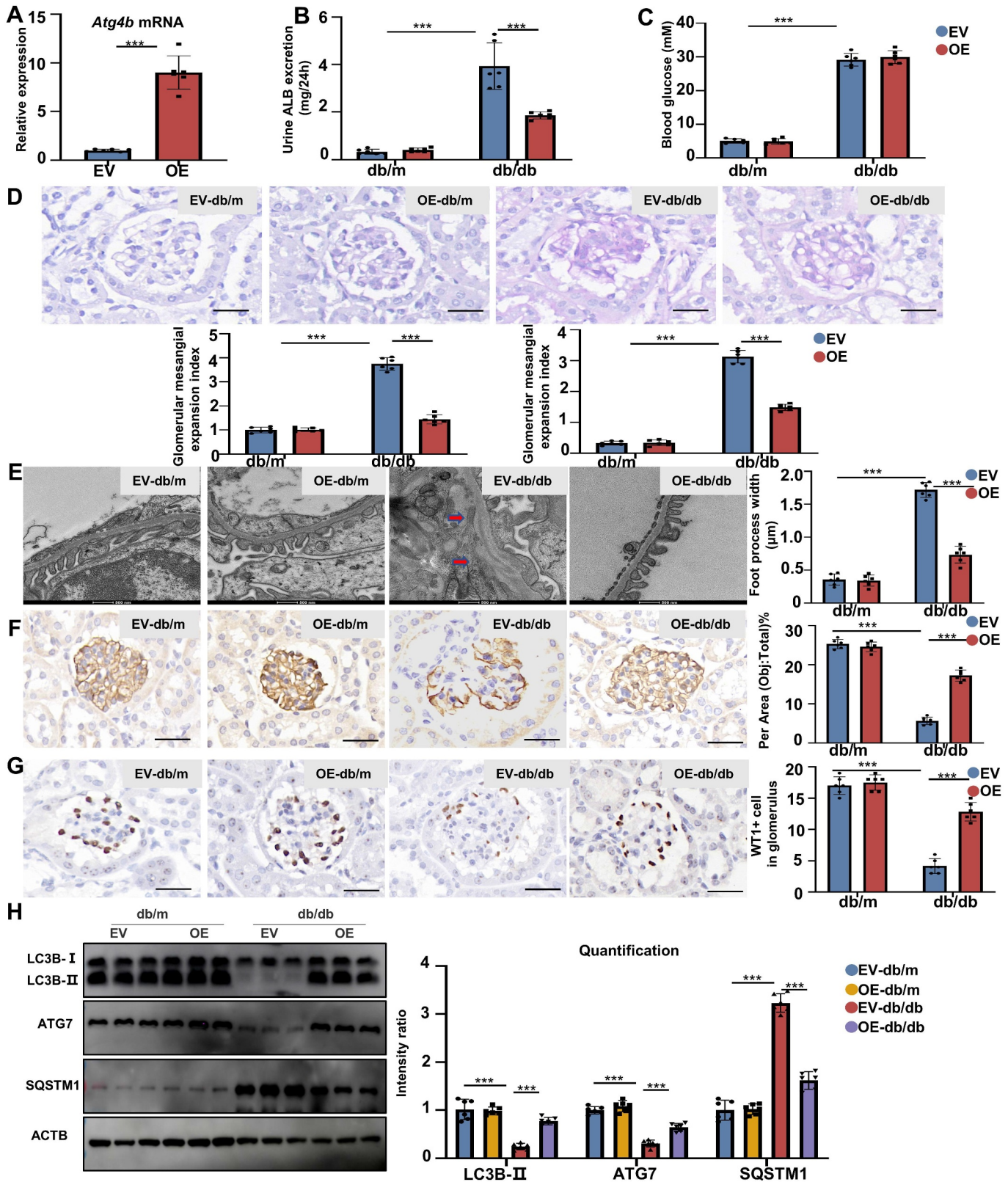
Figure 15. Overexpression of *Atg4b* mitigated kidney damage in db/db type 2 diabetic mice. (A) real-time PCR validated the overexpression efficiency of *Atg4b*. (B) overexpression *Atg4b* could reverse the 24 h urinary ALB excretion rate of db/db mice. (C) overexpression of *Atg4b* had no significant effect on blood glucose. (D) PAS staining showed typical glomerular structural changes in different groups of mice. Scale: 25 μm. (E) the mean thickness of GBM and the mean width of foot process of mice were measured by TEM. Scale: 500 nm. (F and G) immunohistochemistry showed the expression of WT1 and NPHS1. Scale: 25 μm. (H) Western blot showed the expression of autophagy related proteins in the kidney. Abbreviation: EV: empty vector, OE: overexpression. **$p < 0.01$, ***$p < 0.001$.

To the best of our knowledge, this research was the first to reveal that METTL3-mediated m6A methylation of circRNA in DN. Similar to mRNA, m6A is also the most abundant apparent transcriptome modification within circRNA [45]. From the perspective of generation mechanism, the m6A modification of circRNA was mainly added by m6A modification methylase METTL3 and METTL14, and was reversibly removed by the demethylase FTO and ALKBH5 [46]. In addition to the classical function of regulating the stability of circRNAs, m6A modification can affect the function of circRNAs as miRNA sponges by regulating the interaction between circRNAs and miRNAs or affect the interaction between circRNAs and RNA-binding proteins [47]. According to Chen et al., m6A modification in colorectal carcinoma (CRC) cells mediates the cytoplasmic output of a crucial oncogenic called *circNSun2* [24]. However, the regulation of circRNAs by m6A in DN remains unclear. In our research, we identified a regulatory mechanism of *circ -0,000,953*: METTL3-mediated m6A methylation of *circ -0,000,953* was increased which in turn recruited the m6A reader protein YTHDF2 to induce the degradation of *circ -0,000,953*. This finding indicated an important role of m6A in the biological functions of circRNAs.

In conclusion, this study revealed that *circ -0,000,953* regulated autophagy dysfunction and renal injury by acting as an *Mir665-3p* sponge to improve the expression of *Atg4b* *in vitro* and *in vivo*, and METTL3 increased the m6A modification level of *circ -0,000,953* in podocytes through a YTHDF2-dependent mechanism. These results suggest that *circ -0,000,953* is an effective therapeutic target for DN.

Materials and methods

Chemicals and reagents

Lipofectamine RNAiMAX (Invitrogen Life Technologies 13,778–030) was used for transfection. The following antibodies were used: anti-ACTB/β-actin (Proteintech Group, HRP-60008), anti-m6A (Synaptic Systems, 202,003), anti-RELA/NFKB p65 (Cell Signalling Technology, 8242), anti-phospho-RELA/NFKB p65 (Cell Signalling Technology 76,778), anti-WT1 (Abcam, ab267377), anti-NPHS1/Nephrin (Abcam, ab227806), anti-SYNPO/synaptopodin (Santa Cruz Biotechnology, ABN481), anti-MAP1LC3B/LC3B/microtubule associated protein 1 light chain 3 (Cell Signalling Technology 12,741), anti-ATG7 (Abcam, ab133528), anti-ATG4B (Abcam, ab199537), anti-SQSTM1/p62/sequestosome 1 (Abcam, ab109012), anti-MTOR (Proteintech Group 66,888), anti-phospho-MTOR (Proteintech Group 67,778) and anti-TNF (Servicebio, GB11188). Ad-mCherry-GFP-LC3B adenovirus (Beyotime Biotechnology, C3011) was used to detect autophagy flux. STZ was purchased from Sigma-Aldrich (V900890).

Animal studies

All animal experiments were approved by the Animal Research Ethics Committee of Anhui Medical University (No: 20200790) (Hefei, China) and all mice were housed under a specific pathogen-free (SPF) environment in the Animal Laboratory of Anhui Medical University. Male C57BL/6J mice aged 6–8 weeks were purchased from the Laboratory Animal Centre of Anhui Medical University. After 7 days of adaptive feeding, to induce type 1 diabetes mellitus (T1D), 50 mg/kg STZ dissolved in 0.1 M citric acid buffer was intraperitoneally injected into mice after 12 h of fasting daily for 5 consecutive days. After 3 days, the 100 UL titer of 1×10^{12} virus was injected into the tail vein using an insulin needle. One week after the last time of STZ injection, fasting blood glucose levels of >16.7 mmol/L certified the successful build of diabetic models. Mice with T1D were randomly divided into following groups ($n = 6$–8) as follows: Adeno-associated virus 9 (AAV9)-scramble-control, AAV9-shRNA-control, AAV9-scramble-STZ and AAV9-shRNA-STZ groups (Hanbio Biotechnology, Shanghai). We chose db/db mice (aged 4–5 weeks, GemPharmatech, Nanjing, China) as spontaneous T2D (type 2 diabetes mellitus) mice. After 7 days of adaptive feeding, the 100 UL titer of 1×10^{12} virus was injected into the tail vein using an insulin needle. Mice with T2D were randomly divided into following groups ($n = 6$–8) as follows and fed for 16 weeks: AAV9-scramble-db/m, AAV9-shRNA-db/m, AAV9-scramble-db/db and AAV9-shRNA-db/db groups (Hanbio Biotechnology, Shanghai). Establish induced T2D mice model by feeding mice with a high-fat diet (HFD) followed by a single intraperitoneal injection of STZ as previously reported [48,49]. Male C57BL/6 mice (6 weeks old) were fed ND (12.8% kilocalories: fat, 5%; protein, 23%; carbohydrate, 55%) or HFD (fat, 60%; carbohydrate, 20%; protein, 20%) (Trophic Animal Feed High-tech Co. Ltd., TP23400) for 6 weeks. HFD and control groups were administered a high dose of STZ (STZ; 100 mg/kg, intraperitoneal injection, once) and vehicle (citrate buffer). Mice continued to be maintained on a HFD or a ND diets for another 12 weeks. Fasting blood glucose levels were tested weekly in all groups after mice fasting for 12 h. Urine samples were collected for 24 h using metabolic cages. Blood and kidney tissue were collected for further study. All mice were euthanized humanely under anesthesia.

Conditional knockin (cKI) of *circ -0,000,953* in mouse podocytes

Podocytes cKI of *circ -0,000,953* in mice aged 6–8 weeks were purchased from GemPharmatech Co., Ltd. (Nanjing, China) to establish mouse models with conditional knockin of *circ -0,000,953* in podocytes. The *circ -0,000,953*$^{KI/KI}$ mice were established by GemPharmatech. *Nphs2*-Cre *circ -0,000,953*$^{KI/KI}$ (cKI) mice were generated by crossing *circ -0,000,953*$^{KI/KI}$ mice with mice expressing Cre recombinase (Cre) under the regulate of the *Nphs2* promoter (*Nphs2*-Cre). The CAG pro-

moter was used to activate the overexpression of *mmu_-circ_0000953*, and loxp-stop-loxp and EGFP were added before and after *mmu_circ_0000953*, respectively. After propagation with *Nphs2*-cre mice, the stop sequence between two loxp sites was deleted, and *mmu_circ_0000953* and EGFP were expressed. The CRISPR-Cas9 technique was used to microinject sgRNA, cas9 protein and donor into fertilised eggs of C57BL/6JGpt mice to gain positive F0 mice, which were used to reproduce stable F1 offspring. Wild-type (*WT*) and mutant mice were divided into eight groups (*n* = 6–8) as follows: *WT*-control, *Nphs2*-Cre *circ -0,000,953* $^{KI/KI}$-control, *WT*-STZ and *Nphs2*-Cre *circ -0,000,953* $^{KI/KI}$-STZ groups; *WT*-ND, *Nphs2*-Cre *circ -0,000,953* $^{KI/KI}$-ND, *WT*-HFD and *Nphs2*-Cre *circ -0,000,953* $^{KI/KI}$-HFD groups.

Generation of podocyte-specific mettl3 knockout mice and mettl3-KO podocytes

The *mettl3* conditional knockout (cKO) mice were generated and verified as described previously [2]. CRISPR-Cas9 knockout of *Mettl3* in MPC5 was testified as we previously reported [2].

Human renal biopsy samples

Clinical study was carried out in accordance with the principles of the Declaration of Helsinki after obtaining the informed consent of patients. All clinical experiments were sanctified by the Ethics Committee of Anhui Medical University (No: 20200017) (Hefei, China). Kidney biopsy samples of patients with DN and paracancerous (healthy) samples of patients with renal cancer were collected after the patients had signed an informed consent form. These patients were undergoing treatment at the Department of Nephropathy, the First Affiliated Hospital of Anhui Medical University. Patients with T1D and T2D were chose based on the following inclusion criteria: (1) The pathological diagnosis of renal puncture was consistent with the diagnostic criteria of DN; (2) 24 h urine ALB protein levels were >30 mg/24 h; (3) Fasting blood glucose levels were ≥7.0 mmol/L in two tests, random blood glucose levels were ≥11.1 mmol/L in two tests, fasting blood glucose levels in OGTT were ≥7.0 mmol/L, 2-h postprandial blood glucose levels were ≥11.1 mmol/L or glycosylated hemoglobin levels were ≥ 6.5%. Patients with the following criteria were excluded: infection or stress; severe cardiovascular diseases such as cardiac insufficiency, malignant hypertension and arrhythmia; autoimmune diseases; and cancer. Paracancerous kidney tissues collected from patients with kidney cancer served as control samples. Patients with diabetes or other kidney diseases were excluded. The data of patients with DN are shown in Table S1.

Cell culture

Mouse podocyte clone 5 (MPC5) was a kind gift from Prof. Pin-Lan Li (Department of Pharmacology, Virginia Commonwealth University, USA). Mouse tubular epithelial cells (MTECs) (Procell, CP-M062), mouse mesangial cells (SV40) (Procell, CL-0470) and vascular endothelial cells (VECs) (Procell, CP-M060) were cultured in low-glucose DMEM (Gibco,11885092) with 10% fetal bovine serum (Gibco,10270–106). To ensure cell proliferation, MPC5 cells were cultured in low-glucose DMEM containing 20-U/mL mouse recombinant IFNG (PeproTech, 315–05) at 33°C. To induce cell differentiation, MPC5 cells were cultured for 7 days at 37°C without IFNG. The cells were stimulated with 30 mM glucose or 200 ng/mL rapamycin (MCE Technology, HY-10219) or 1 μM bafilomycin A$_1$ (MCE Technology, HY-100558) for 24 h after adaptive culture.

Cell transfection

Cells were transfected with lentiviruses (Genechem Biotechnology, China) and incubated at 37°C overnight. Continue the culture for 24 h and replace the medium containing the virus with fresh medium. Overexpressed plasmids or siRNAs (Hanbio Biotechnology, China) were transfected using the Lipofectamine RNAiMAX reagent (Invitrogen Life Technologies 13,778,075) (the sequences of siRNA used in this study are shown in Table S2). A negative empty vector served as the control. OPTI-MEM (Invitrogen Life Technologies 31,985,062) mixed with Lipofectamine RNAiMAX and siRNAs or plasmids was incubated for 15 min and subsequently added to cells. After of incubation for 4–6 h, OPTI-MEM was discarded and replaced with a complete medium containing serum. The efficiency of transfection was analyzed via real-time PCR, and monoclonal was selected for subsequent amplification.

Western blot

Proteins were extracted from lysed cells and tissues with radio-immunoprecipitation assay (RIPA) buffer (Beyotime Biotechnology, P0013B) with protease (Beyotime Biotechnology, P1005) and phosphatase (Beyotime Biotechnology, P1082) inhibitors, and the concentrations of protein were tested by a bicinchoninic acid (BCA) assay kit (Beyotime Biotechnology, P0012). After the extracted proteins were denatured at 100°C for 10 min, they were subjected to electrophoresis, transferred onto a membrane, and incubated with the specific antibodies. Protein blot was developed using an enhanced chemiluminescent (ECL) substrate kit (Thermo Fisher Scientific 32,106) and a gel imaging system (Bio-Rad, USA).

Immunohistochemistry

Tissue section was dewaxed, incubated with H$_2$O$_2$, repaired in fresh citrate solution under high pressure and incubated with goat serum (Beyotime Biotechnology, C0265) for 30 min. The goat serum on the surface of the slide was removed, and primary antibodies were added overnight. Thereafter, kidney tissue was incubated with a secondary antibody and stained with DAB. Nuclei was stained with hematoxylin for 3 min and photographed using the positive microscope (Germany, Zeiss).

RNA extract and real-time PCR

Cells and tissues RNA was extracted using the TRIzol reagent (Invitrogen Life Technologies 15,596,026), quantified on

a Nanodrop-6000 system and reverse transcribed using 4×Hifair®III SuperMix plus on a thermal cycler system (CFX-6, Bio-Rad, CA, USA). *Actb/β-actin* was used as a reference gene for normalizing data. The relevant primers used for PCR are shown in Table S3. Sequences of Mir-specific primers and reverse primers are shown in Table S4.

Glomerulus separation

Hanks' solution (Gibco 13,150,016) was added to kidney cortex tissue. The tissue sample was initially screened on an 80-mesh stainless steel copper mesh (Solarbio, YA0944), and the sifted kidney tissue sample was subsequently filtered on a 120-mesh screen (Solarbio, YA0946). The sample was washed with Hanks' solution to remove tissue mass and placed on a 200-mesh screen (Solarbio, YA0949) for further filtration. Finally, the glomerulus on the strainer was collected and lysed for subsequent experiments.

Circular RNA sequencing

Kidney RNA was extracted from the kidney cortex tissue. mRNA was enriched with magnetic beads with oligo (dT) and incubated with a fragmentation buffer. The resulting mRNA fragment was used as templates. The first cDNA strand was synthesized using six-base random hexamers, whereas the second strand was synthesized using a buffer solution, dNTPs, Rnase H and DNA polymerase I. These strands were purified using the QiaQuick PCR kit (Qiagen 28,104) and eluted with an EB buffer solution. After terminal repair, base A and sequencing joint were added, and the target fragments were recovered via agarose gel electrophoresis and amplified via PCR to complete the preparation of the whole library. The constructed library was sequenced on the Illumina HiSeqTM 4000 platform. Anchor read was mapped to the genome, and the results were submitted to the UROBORUS software for identifying circRNAs. The libraries were constructed, validated and sequenced at Origin Biotech (Shanghai, China).

RNA-sequencing

Dynabeads Oligo (dT) beads (Thermo Fisher Scientific, 25–61005,) were used for specifically capturing mRNAs containing polyadenylate (polyA) through two rounds of purification. The captured mRNAs were fragmented at the high temperature by the NEBNextR Magnesium RNA Fragmentation Module (E6150S). cDNA was synthesized using reverse transcriptase. *E. coli* DNA polymerase I (NEB, m0209) and Rnase H (NEB, m0297) were subsequently synthesized. The two-strand library was digested in the UDG enzyme (NEB, m0280) and pre-denatured through PCR to form fragments with a size of 300 bp ± 50 bp (chain-specific library). The Illumina Novaseq^{TM} 6000 platform (LC Bio Technology Co., Ltd., Hangzhou, China) was used for double-end sequencing in the PE150 mode according to standard protocols. The libraries were constructed, validated, and sequenced at OE Biotech (Shanghai, China).

Fluorescence in situ hybridisation (FISH)

Fluorescently labeled nucleic acid probes specific to *circ-0,000,953* and *Mir665-3p* were used for hybridization. Samples were fixed with 4% paraformaldehyde and cleaned by hydrochloric alcohol. The samples were incubated at 46°C, allowed to dry for 10 min, successively immersed in a gradient ethanol, dehydrated for 5 min. Thereafter, 10 μL of a pre-configured hybridization buffer and 1 μL of the probe were added. The washing buffer was sealed, incubated in dark, hybridized at 46°C for 1.5 h and preheated to 48°C, and slide was incubated at 48°C for 30 min after hybridization. The slides were washed with pure water and incubated with an anti-fading reagent. The expression positions of *circ-0,000,953* and *Mir665-3p* were observed using a laser confocal microscope (OLYMPUS IX83, Japan). The probe sequences were shown in Table S5.

Affinity-isolation assay

A biotin-labeled *circ-0,000,953* probe was synthesized and used to bind to the *circ-0,000,953* junction site. MPC5 cells were incubated with 4 μg of the biotinylated probe for 4–6 h. Hifair® Streptavidin Magnetic Beads (Thermo Fisher Scientific 88,816) were prepared and incubated with Rnase-free bovine serum ALB (10 mg/mL; Thermo Fisher Scientific, AM2616) and 10 μL of tRNA (10 mg/mL; Thermo Fisher Scientific, AM7119) incubated in a dissolved buffer for 3 h to reduce nonspecific binding. The beads were used to pull down the biotin-coupled RNA complex and incubated on a shaker overnight at 4°C. The magnetic beads were washed thrice and the expression of miRNAs were detected via real-time PCR. The probe sequences used in this study were shown in Table S6.

Rnase R and actinomycin D treatment

Total RNA was incubated with Rnase R (Epicentre Technologies, RNR07250) (20 U/μL) at 37°C for 10–30 min. After RNA digestion, reverse transcription was directly performed. Podocytes were incubated with actinomycin D (5 μg/mL; Cell Signaling Technology, 50-76-0) to stop transcription, and *circ-0,000,953* and its parent genes were detected. Samples were collected at 0, 6, 12 and 24 h after actinomycin D treatment. The expression of *circ-0,000,953* and its parent genes were detected via real-time PCR.

Luciferase reporter assay

Circ-0,000,953 sequence including target site for the miRNA candidate was synthesized and cloned downstream in a *pSI-Check2* reporter vector (Promega, C8021). A luciferase version of mutant version of *circ-0,000,953* (*pSI-Check2-circ-0,000,953-mutant*), *circ-0,000,953* (*pSI-Check2-circ-0,000,953-wildtype*), mutant version of *Atg4b* (*pSI-Check2-Atg4b-mutant*), and luciferase version of *Atg4b* (*pSI-Check2-Atg4b-wildtype*) were designed by deleting the corresponding complementary sites. The reporter vector, *Mir665-3p* mimic or negative control was transfected into MPC5 cells by Lipofectamine RNAiMAX (Invitrogen Life Technologies, 13,

778–030). The activity of firefly and Renilla luciferase was detected by a dual-luciferase system (Promega, E1910) followed the instructions.

Statistical analysis

All data were expressed as the mean ± standard deviation (SD). Unpaired t-test or one-way analysis of variance were performed using the GraphPad Prism 8 software. All experiments were independently performed in triplicate. A p-value of < 0.05 was considered statistically significant.

Disclosure statement

No potential conflict of interest was reported by the authors.

ORCID

Yonggui Wu http://orcid.org/0000-0001-6434-4759

References

[1] Azushima K, Gurley SB, Coffman TM. Modelling diabetic nephropathy in mice. Nat Rev Nephrol. 2018 Jan;14(1):48–56. doi: 10.1038/nrneph.2017.142

[2] Jiang L, Liu X, Hu X, et al. METTL3-mediated m(6)A modification of TIMP2 mRNA promotes podocyte injury in diabetic nephropathy. Mol Ther. 2022 Apr 6;30(4):1721–1740. doi: 10.1016/j.ymthe.2022.01.002

[3] Liu M, Liang K, Zhen J, et al. Sirt6 deficiency exacerbates podocyte injury and proteinuria through targeting notch signaling. Nat Commun. 2017 Sep 4;8(1):413. doi: 10.1038/s41467-017-00498-4

[4] Yasuda-Yamahara M, Kume S, Tagawa A, et al. Emerging role of podocyte autophagy in the progression of diabetic nephropathy. Autophagy. 2016;11(12):2385–2386. doi: 10.1080/15548627.2015.1115173

[5] Lenoir O, Jasiek M, Henique C, et al. Endothelial cell and podocyte autophagy synergistically protect from diabetes-induced glomerulosclerosis. Autophagy. 2015;11(7):1130–1145. doi: 10.1080/15548627.2015.1049799

[6] Dolai S, Takahashi T, Qin T, et al. Pancreas-specific SNAP23 depletion prevents pancreatitis by attenuating pathological basolateral exocytosis and formation of trypsin-activating autolysosomes. Autophagy. 2020;17(10):3068–3081. doi: 10.1080/15548627.2020.1852725

[7] Dolai S, Liang T, Orabi AI, et al. Pancreatitis-induced depletion of syntaxin 2 promotes autophagy and increases basolateral exocytosis. Gastroenterology. 2018;154(6):1805–1821.e5. doi: 10.1053/j.gastro.2018.01.025

[8] Jin J, Shi Y, Gong J, et al. Exosome secreted from adipose-derived stem cells attenuates diabetic nephropathy by promoting autophagy flux and inhibiting apoptosis in podocyte. Stem Cell Res Ther. 2019;10(1). doi: 10.1186/s13287-019-1177-1

[9] Barutta F, Bellini S, Kimura S, et al. Protective effect of the tunneling nanotube-TNFAIP2/M-sec system on podocyte autophagy in diabetic nephropathy. Autophagy. 2023 Feb;19(2):505–524. doi: 10.1080/15548627.2022.2080382

[10] Yang H, Xie T, Li D, et al. Tim-3 aggravates podocyte injury in diabetic nephropathy by promoting macrophage activation via the NF-κB/TNF-α pathway. Mol Metabol. 2019;23:24–36. doi: 10.1016/j.molmet.2019.02.007

[11] Xiao Y, Zhou Y, Lu Y, et al. PHB2 interacts with LC3 and SQSTM1 is required for bile acids-induced mitophagy in cholestatic liver. Cell Death Dis. 2018;9(2). doi: 10.1038/s41419-017-0228-8

[12] Li A, Yi B, Han H, et al. Vitamin D-VDR (vitamin D receptor) regulates defective autophagy in renal tubular epithelial cell in streptozotocin-induced diabetic mice via the AMPK pathway. Autophagy. 2021;18(4):877–890. doi: 10.1080/15548627.2021.1962681

[13] Liu XQ, Jiang L, Li YY, et al. Wogonin protects glomerular podocytes by targeting bcl-2-mediated autophagy and apoptosis in diabetic kidney disease. Acta Pharmacol Sin. 2021 Jul 12;43(1):96–110. doi: 10.1038/s41401-021-00721-5

[14] Liu N, Xu L, Shi Y, et al. Podocyte autophagy: a potential therapeutic target to prevent the progression of diabetic nephropathy. J Diabetes Res. 2017;2017:1–6. doi: 10.1155/2017/3560238

[15] Zhou L, Liu Y. Wnt/β-catenin signalling and podocyte dysfunction in proteinuric kidney disease. Nat Rev Nephrol. 2015;11(9):535–545. doi: 10.1038/nrneph.2015.88

[16] Li Y, Pan Y, Cao S, et al. Podocyte EGFR inhibits autophagy through upregulation of rubicon in type 2 diabetic nephropathy. Diabetes. 2021 Feb;70(2):562–576. doi: 10.2337/db20-0660

[17] Qi W, Keenan HA, Li Q, et al. Pyruvate kinase M2 activation may protect against the progression of diabetic glomerular pathology and mitochondrial dysfunction. Nat Med. 2017 Jun;23(6):753–762. doi: 10.1038/nm.4328

[18] Huang R, Zhang Y, Han B, et al. Circular RNA HIPK2 regulates astrocyte activation via cooperation of autophagy and ER stress by targeting MIR124-2HG. Autophagy. 2017 Oct 3;13(10):1722–1741. doi: 10.1080/15548627.2017.1356975

[19] Qu S, Yang X, Li X, et al. Circular RNA: a new star of noncoding RNAs. Cancer Lett. 2015 Sep 1;365(2):141–148. doi: 10.1016/j.canlet.2015.06.003

[20] Han B, Chao J, Yao H. Circular RNA and its mechanisms in disease: from the bench to the clinic. Pharmacol Ther. 2018 Jul;187:31–44. doi: 10.1016/j.pharmthera.2018.01.010

[21] Patop IL, Kadener S. circRNAs in Cancer. Curr Opin Genet Dev. 2018 Feb;48:121–127. doi: 10.1016/j.gde.2017.11.007

[22] Xu Z, Li P, Fan L, et al. The potential role of circRNA in tumor Immunity regulation and immunotherapy. Front Immunol. 2018;9:9. doi: 10.3389/fimmu.2018.00009

[23] Memczak S, Jens M, Elefsinioti A, et al. Circular RNAs are a large class of animal RNAs with regulatory potency. Nature. 2013 Mar 21;495(7441):333–338. doi: 10.1038/nature11928

[24] Chen RX, Chen X, Xia LP, et al. N(6)-methyladenosine modification of circNSUN2 facilitates cytoplasmic export and stabilizes HMGA2 to promote colorectal liver metastasis. Nat Commun. 2019 Oct 16;10(1):4695. doi: 10.1038/s41467-019-12651-2

[25] Shang FF, Luo L, Yan J, et al. CircRNA_0001449 disturbs phosphatidylinositol homeostasis and AKT activity by enhancing Osbpl5 translation in transient cerebral ischemia. Redox Biol. 2020 Jul;34:101459. doi: 10.1016/j.redox.2020.101459

[26] Lu C, Chen B, Chen C, et al. CircNr1h4 regulates the pathological process of renal injury in salt-sensitive hypertensive mice by targeting miR-155-5p. J Cell Mol Med. 2020 Jan;24(2):1700–1712. doi: 10.1111/jcmm.14863

[27] Luan J, Jiao C, Kong W, et al. circHLA-C plays an important role in lupus nephritis by sponging miR-150. Mol Ther Nucleic Acids. 2018 Mar 2;10:245–253.

[28] Xiong Y, Zhang J, Song C. CircRNA ZNF609 functions as a competitive endogenous RNA to regulate FOXP4 expression by sponging miR-138-5p in renal carcinoma. J Cell Physiol. 2019 Jul;234(7):10646–10654. doi: 10.1002/jcp.27744

[29] Kolling M, Seeger H, Haddad G, et al. The Circular RNA ciRs-126 predicts survival in critically ill patients with acute kidney injury. Kidney Int Rep. 2018 Sep;3(5):1144–1152. doi: 10.1016/j.ekir.2018.05.012

[30] Chen B, Li Y, Liu Y, et al. circLRP6 regulates high glucose-induced proliferation, oxidative stress, ECM accumulation, and inflammation in mesangial cells. J Cell Physiol. 2019 Nov;234(11):21249–21259. doi: 10.1002/jcp.28730

[31] Peng F, Gong W, Li S, et al. circRNA_010383 acts as a sponge for miR-135a, and its downregulated expression contributes to renal fibrosis in diabetic nephropathy. Diabetes. 2021 Feb;70 (2):603–615. doi: 10.2337/db20-0203

[32] Qin X, Zhao Y, Gong J, et al. Berberine protects glomerular podocytes via inhibiting Drp1-mediated mitochondrial fission and dysfunction. Theranostics. 2019;9(6):1698–1713. doi: 10.7150/thno.30640

[33] Yang D, Livingston MJ, Liu Z, et al. Autophagy in diabetic kidney disease: regulation, pathological role and therapeutic potential. Cell Mol Life Sci. 2018 Feb;75(4):669–688. doi: 10.1007/s00018-017-2639-1

[34] Sakai S, Yamamoto T, Takabatake Y, et al. Proximal Tubule Autophagy Differs in Type 1 and 2 Diabetes. J Am Soc Nephrol. 2019 Jun;30(6):929–945. doi: 10.1681/ASN.2018100983

[35] Zhang C, Li W, Wen J, et al. Autophagy is involved in mouse kidney development and podocyte differentiation regulated by notch signalling. J Cell Mol Med. 2017 Jul;21(7):1315–1328. doi: 10.1111/jcmm.13061

[36] Yao R-Q, Ren C, Xia Z-F, et al. Organelle-specific autophagy in inflammatory diseases: a potential therapeutic target underlying the quality control of multiple organelles. Autophagy. 2020;17 (2):385–401. doi: 10.1080/15548627.2020.1725377

[37] Wei TT, Yang LT, Guo F, et al. Activation of GPR120 in podocytes ameliorates kidney fibrosis and inflammation in diabetic nephropathy. Acta Pharmacol Sin. 2021 Feb;42(2):252–263. doi: 10.1038/s41401-020-00520-4

[38] Gurley SB, Ghosh S, Johnson SA, et al. Inflammation and immunity pathways regulate genetic susceptibility to diabetic nephropathy. Diabetes. 2018 Oct;67(10):2096–2106. doi: 10.2337/db17-1323

[39] Cheng Q, Pan J, Zhou ZL, et al. Caspase-11/4 and gasdermin D-mediated pyroptosis contributes to podocyte injury in mouse diabetic nephropathy. Acta Pharmacol Sin. 2021 Jun;42 (6):954–963. doi: 10.1038/s41401-020-00525-z

[40] Bhatt K, Lanting LL, Jia Y, et al. Anti-inflammatory role of MicroRNA-146a in the pathogenesis of diabetic nephropathy. J Am Soc Nephrol. 2016 Aug;27(8):2277–2288. doi: 10.1681/ASN.2015010111

[41] Wang W, Ying Y, Xie H, et al. miR-665 inhibits epithelial-to-mesenchymal transition in bladder cancer via the SMAD3/SNAIL axis. Cell Cycle. 2021 Jul;20(13):1242–1252. doi: 10.1080/15384101.2021.1929677

[42] Liu S, Li XM, Yuan JB, et al. MiR-665 inhibits inflammatory response in microglia following spinal cord injury by targeting TREM2. Eur Rev Med Pharmacol Sci. 2021 Jan;25(1):65–70. doi: 10.26355/eurrev_202101_24349

[43] Chen T, Liang Q, Xu J, et al. MiR-665 regulates vascular smooth muscle Cell senescence by interacting with LncRNA GAS5/SDC1. Front Cell Dev Biol. 2021;9:700006. doi: 10.3389/fcell.2021.700006

[44] Guo Q, Lin Y, Hu J. Inhibition of miR-665-3p enhances autophagy and alleviates inflammation in Fusarium solani-induced keratitis. Invest Ophthalmol Vis Sci. 2021 Jan 4;62(1):24. doi: 10.1167/iovs.62.1.24

[45] Di Timoteo G, Dattilo D, Centron-Broco A, et al. Modulation of circRNA metabolism by m(6)A modification. Cell Rep. 2020 May 12;31(6):107641. doi: 10.1016/j.celrep.2020.107641

[46] Chen YG, Chen R, Ahmad S, et al. N6-Methyladenosine Modification Controls Circular RNA Immunity. Mol Cell. 2019 Oct 3;76(1):96–109 e9. doi: 10.1016/j.molcel.2019.07.016

[47] Wang J, Ishfaq M, Xu L, et al. METTL3/m(6)A/miRNA-873-5p attenuated oxidative stress and apoptosis in colistin-induced kidney injury by modulating Keap1/Nrf2 pathway. Front Pharmacol. 2019;10:517. doi: 10.3389/fphar.2019.00517

[48] Gao L, Yang T-T, Zhang J-S, et al. THBS1/CD47 modulates the interaction of γ-catenin with E-cadherin and participates in epithelial–mesenchymal transformation in lipid nephrotoxicity. Front Cell Dev Biol. 2021;8: doi: 10.3389/fcell.2020.601521

[49] Han Y-C, Tang S-Q, Liu Y-T, et al. AMPK agonist alleviate renal tubulointerstitial fibrosis via activating mitophagy in high fat and streptozotocin induced diabetic mice. Cell Death Dis. 2021;12(10). doi: 10.1038/s41419-021-04184-8